International Journal of Robotics and Control Systems
Vol. 3, No. 4, 2023, pp. 1021-1060
ISSN 2775-2658
http://pubs2.ascee.org/index.php/ijrcs

Dynamic Performance Enhancement of a Self-Excited Induction Generator Connected to the Grid Using an Effective Control Algorithm

Asmaa Saleh [a,1], Ahmed A. Zaki Diab [a,2], Ahmed A. M. El-Gaafary [a,3], Mahmoud A. Mossa [a,4,*]

[a] Electrical Engineering Department, Faculty of Engineering, Minia University, Minia 61111, Egypt
[1] semsemsaleh47@gmail.com; [2] a.diab@mu.edu.eg; [3] elgaafary@mu.edu.eg; [4] mahmoud_a_mossa@mu.edu.eg
* Corresponding Author

ARTICLE INFO

Article history
Received September 26, 2023
Revised November 28, 2023
Accepted December 29, 2023

Keywords
SEIG;
Nonlinear Control;
Predictive Control;
Ripples;
Dynamic Response

ABSTRACT

The current study aims to present a comprehensive analysis of a control technique used for improving the dynamic performance of a grid connected self-excited induction generator (SEIG). All components in the control system are modelled and explained in details. The management of SEIG operation is achieved through controlling the machine side converter using a new formulated predictive voltage control scheme (PVC). The proposed (PVC) is compared to field oriented control (FOC), model predictive current control (MPCC) and model predictive direct torque control (MPDTC) systems. MPDTC and MPCC have several drawbacks like high ripple, high load commutation, and using a weighting factor in their cost function, While FOC systems depend on machine parameters for variable estimation factors, need to use PI regulators and co-ordinate transformations, which complicate the system and slow down the dynamic response. The results obtained indicate that the proposed PVC is effective, as the ripples are reduced by 43% when compared to the MPDTC-used one and by 30% when compared to MPCC. Additionally, PVC's time response is less than that of the FOC by 15%, MPCC by 9%, and MPDTC by 4%. Furthermore, PVC produces 38% fewer commutations than MPCC and 40% fewer commutations than MPDTC. Consequently, the generator's efficiency and dependability both increased as a result of its better performance.

1. Introduction

The main issues affecting the energy industry in the world today are the continuing increase in energy consumption in all of its forms and the associated pollution impacts, which are mostly brought on by the combustion of fossil fuels. The growing need for clean energy in our daily life compels developers to consider novel control strategies to maximize the power extraction from renewable energy sources like wind, geothermal, solar, and wave energies [1], [2].

With the development of renewable energy power generation [9], The SEIG's widely adopted [7], [8], as the advantages of this generator over synchronous generator [4], are brushless construction with squirrel-cage rotor, smaller size and weight, lower maintenance cost, ease of construction, no DC supply for excitation and better transient performance, (SEIG) is widely

employed in standalone systems especially in hydroelectric, tidal, wind power plants and other renewable energy sources, where most of them are located in remote areas or developing countries [3].

However, the main drawback of the SEIG system is that it produces very dynamic voltage and frequency under varying load conditions. Although several research have concentrated on controlling the voltage and frequency of the SEIG system under varied loads, the machine's nonlinear behavior means that the control of speed and voltage does not produce a suitable level of performance [13]-[15]. Alternatively, the required magnetization can be provided to the SEIG from the grid under the direct link between the generator and the utility grid. In this case, a control system must be present to manage the grid power to maintain a unity power factor operation and regulate the DC link voltage as well. However, the primary disadvantage of SEIG is its inherently poor voltage regulation. Having a suitable voltage regulation method becomes important as a result. Researchers have worked hard to present several SEIG models [17]-[19].

In Ref. [17] investigated the steady state performance of SEIG using the d-q model. In Ref. [18] replaced the piecewise linear approximation of the nonlinear magnetizing reactance of the induction generator with an artificial neural network (ANN) in order to identify the generated frequency during steady-state operation of the SEIG. Although Artificial Neural Networks have been shown to be more accurate than piecewise linear approximations in capturing the magnetizing behavior of Induction Generators, finding generated frequency via iterative techniques is time-consuming and to some extent erroneous. In Ref. [19] used MATLAB's Quasi-Newton optimization, Genetic Algorithm, and Pattern Search tools to perform the steady-state analysis. Researchers have also developed various control methods to improve dynamic performance of SEIG, and then testify them with the SEIG due to the SEIG's many benefits as a generation unit.

There are many different ways to control SEIG [11], [45], but one of the trickiest parts of the generating system is Fig.uring out which control is best. Due to their ease of usage, field-oriented control (FOC) and direct torque control (DTC) are thought to be the most often utilized SEIG control techniques. Through the use of two distinct inner current loops (PI), FOC independently controls torque and flux, as well as active and reactive, as demonstrated by its ability to reduce ripples, have a smooth dynamic response, and control nonlinearities in the generator model. However, the complexity resulting from the use of the coordination transformation, the delay response, and its reliance on the machine parameters as a result of the PI are still major drawbacks of the FOC.

Different variations of the FOC approach have been used depending on the controlling of the DC bus voltage and the rotor flux of SEIG such as in [20]. For a specific range of wind speed oscillations, field oriented control by rotor flux orientation accounting for the cross-effect is proposed in to regulate the DC bus voltage as well as the rotor flux of SEIG.

In order to maintain a constant DC voltage across the capacitor that is equal to the reference value for (SEIG), vector control system is demonstrated using the indirect rotor field-oriented (IRFO) control algorithm. A current-controlled voltage source inverter and a single electrolytic capacitor are used in the system to excite it. No matter how the rotor speed or load change. Two alternative types of fuzzy logic (FL) [44] voltage controllers are presented and examined to accomplish this. By contrasting the created FL voltage controllers' performance with that of the optimally tuned traditional PI controller, their effectiveness is assessed. Various combinations of rotor speed, load, and DC voltage are analyzed on both an experimental and simulation level [23].

In order to maximize power output from a variable wind turbine and to control the DC-link voltage, rotor flux, and AC load voltage in (SEIG) system, an adaptive proportional-integral (API) control method is developed. Since finite time estimators for the unknown time-varying rotor resistance, rotor flux (non-measurable signal), and stator electrical angular position necessary for the online implementation of the proposed algorithm are provided, the resulting controller associated

with the FOC technique can be easily implemented in practice. The computation results were achieved using a wind speed profile that was rather low. As a result, if the wind speed profile is relatively low, the producing system with the suggested control approach is appropriate for the installation of variable wind speed turbines for grid-connected and distant areas [22].

The SEIG experiences a smooth dynamic response as a result of the FOC schemes success in enhancing torque response and minimizing ripples. Although Researchers have worked hard in FOC systems still have several drawbacks, such as the fact that they depend on machine parameters for variable estimation factors. In addition, they need to use PI regulators and coordinate transformations, which complicate the system and slow down the dynamic response. They also need to use a modulation stage.

An attempt to avoid the shortcomings of FOC is DTC [32] which replaced the PI controls with hysteresis comparators Due to a number of benefits of DTC, including good torque control in steady-state and transient operating circumstances, the lack of coordinate transforms and current controllers, fast dynamic response, and less computation effort compared with the FOC [33], the DTC-based WECS is better suitable for low power applications [25]. Comparative studies of indirect vector control (IVC) based Grid-connected SEIG-based Wind Energy Conversion Systems and direct torque control (DTC) using Space Vector Pulse Width Modulation (SVPWM) are shown in [27]. The frequency converter (which also includes a Rotor side Connected Converter (RSCC) and Grid Side Connected Converter (GSCC) controls the torque ripples, rotor speed overshoot, undershoot, active power, reactive power, and DC-Link Voltage. The techniques of Sinusoidal Pulse Width Modulation (SPWM) and Space Vector Pulse Width Modulation (SVPWM) have been proposed for GSCC and RSCC, respectively.

Where the basic principle of SPWM is to vary the width (or duration) of the pulses in the carrier waveform based on the instantaneous amplitude of the reference waveform. When the reference waveform is positive, the pulses in the carrier waveform are generated such that the output voltage or current is positive. By adjusting the pulse width, the average value of the output waveform can be controlled. The modulation index, which is the ratio of the peak amplitude of the reference waveform to the peak amplitude of the carrier waveform, determines the distortion and quality of the output waveform. A higher modulation index generally leads to a waveform with lower harmonic distortion and closer resemblance to a sinusoidal waveform.

(SVPWM) It is a modulation technique commonly used in power electronics for controlling three-phase voltage inverters. Similar to SPWM, SVPWM also aims to generate a desired output voltage waveform by modulating a high-frequency carrier waveform. By using SVPWM, the output voltage waveform can closely approximate a sinusoidal waveform. This modulation technique provides several advantages, including reduced harmonic distortion, improved efficiency, and better utilization of the available voltage. It also allows for precise control of the output voltage and current.

Another approach that follows the same principle of DTC [41] is direct Power Control (DPC) [5], [6] which regulates both active and reactive powers. Because of the established relationship between developed torque and active power, managing active power also affects developed torque, and managing reactive power affects flux. As a result, DPC is regarded as a modification of the DTC strategy.

As a result of academics attempts to think about a new control system that eliminates the disadvantages of FOC Predictive control (PC) [16] was recently discovered. The FOC's PI regulators and current control loops are replaced with a cost function. This has helped to minimize the complexity and ripples, produce a superior steady-state performance, and achieve a quick dynamic response. The selected cost function contains two components that represent the absolute error of the variables that need to be controlled. It also offers the advantage of flexibility and the ability to manage several control objectives at once [34].

To overcome the problems of FOC, DTC, and DPC, A lot of new control schemes were developed recently that seem particularly their significant sensitivity due to torque ripples and generator parameter dependence. For this reason, nonlinear controllers are generally known to be less sensitive to system factors. These methods, including model predictive control (MPC) [12], [42] and sliding mode control (SMC) [35].

Since sliding mode control (SMC) is nonlinear, it is a better method for handling disruptions. In addition to its capacity to handle any existing disturbance or unmolded dynamics, SMC offers a number of advantages, including good dynamic response, high robustness against parameter alterations compared to FOC, reduced ripple compared to DTC and DPC, and simple implementation, in addition to the ability to deal with any existing disturbance or unmolded dynamics Still, certain disadvantages arise, such as chattering occurrences and phase stability issues.

Model predictive control (MPC) [12] is an additional approach to dealing with nonlinearities that aims to solve the limits of the control rule and the linarites of FOC, DTC, and DPC. Currently, MPC is gaining popularity as a method for predicting the behavior of plants in the future and implementing the best control measures in accordance with the predetermined control objectives. MPC has a number of benefits, including the ability to combine control loops into a single loop, ease of application to multivariable systems, and quick dynamic response. Moreover, it simplifies the addition of non that are divided into two topologies. All of this has effectively reduced system complexity, which has sped up system dynamics.

An attempt to preserve the simplicity and eliminate the ripple in traditional DTC is MPDTC which substituting a more flexible cost function that multiplies a weighting factor, but it has a few flaws. First, the cost function needs a weighting factor W_f [30] in order to achieve the desired balance between torque and rotor flux. Additionally, any inaccurate selection of W_f exposes the torque and rotor flux ripples to an increase. Another drawback in MPDTC is that because the cost function's components must be calculated, any variation or change to the model's parameters will affect the estimated variables [36]. Additionally, MPDTC's computational weight is viewed as a problem since it necessitates the estimate and prediction of rotor flux and torque.

Model predictive current control (MPCC) [28], [29], a different PC topology that attempts to fix some of MPDTC's defects, exhibits less torque and flux ripples overall than MPDTC [38]. Additionally, A weighting factor (W_f) is not used in MPCC, which replaces PI current in FOC with a simple cost function that sums the errors between the direct and quadrature stator current. MPCC is seen as a transfer of FOC. Regarding the disposal of the PI regulators [10], which are frequently used by the FOC technique, MPCC and MPDTC are in agreement. The MPCC achieved faster dynamics repose and a simpler constructor, but it has a disadvantage in that the cost function requires estimation and prediction values, meaning that any change in machine parameters will affect the performance.

To achieve a balance between the required computational burden, the design of a cost function and its terms must be properly executed when considering predictive control. We use the PVC which can overcome the shortages of previous predictive control methods like (MPCC, MPDTC) and also the shortages of the FOC.

The proposed PVC provides several advantages such as it uses very simple cost function as it doesn't need to use W_f and consists of the absolute errors between the reference and actual values of stator voltage component help in reducing significantly the complication needed by the predictive controller because:

1. The actual voltage component (u_{ds} and u_{qs}) needed by the cost function can be directly obtain from the switching signals of the inverter after adjusting the finite control set (FCS) which refers to a control strategy that utilizes a finite set of discrete control values or actions instead of using a continuous range of control signals, the FCS operates with a predefined set of discrete

control values. These control values are typically represented by binary codes or digital signals which simplify the control implementation, FCS control can offer fast response times because the discrete control actions can be rapidly switched.

2. Also the reference voltage component (u_{ds}^{*} and u_{qs}^{*}) can be obtain via using a designed (PI) controller which plays a crucial role in maintaining voltage stability and ensuring that the predicted voltage conditions align with the desired set points.

The detailed analysis of the performances prove the effectiveness of the proposed PVC and this is approved through low ripples and low current harmonics, also the reduction in the number of commutation and quick dynamic response.

In brief, the paper's contributions are discussed as follows:

1. The paper contributed detailed design for a complete generation system used the SEIG as a main generation unit.
2. All system components in the generation system are modelled and explained in details.
3. In the paper proposed an effective predictive controller was overcome several disadvantages of previous controller like (FOC) and also other predictive controller like (MPCC) and (MPDTC).
4. The paper introduces a comprehensive analysis for the generator's dynamic performance analysis under various control methods and also provides a detailed comparison study between the performances of all these controllers to validate the effectiveness of the proposed voltage control.
5. The detailed analysis of the performances prove the effectiveness of the proposed PVC and this is shown via the reduction in the generated variable ripples and current harmonics and also the reduction in the no of commutation and quick dynamic response.

The presented study is structured as follows:

Sec. 2 introduces the introduction and the literature review about the previous used controller with SEIG. Sec. 3 introduces the mathematical model for each system component. Section (4) provide the modeling of all control methods (FOC, MPCC, MPDTC and PVC) and their scheme are described in a systematic manner. Sec.5 introduces the test results and its related analysis. Sec. 6 introduces the conclusion and research output

2. System Modeling

2.1. Mathematical Model of SEIG

To understand the dynamic model of SEIG the first step is to convert the 3-phase to 2-phase (d-q) model using Park's transformation.

One of the most common techniques for analyzing induction machines is the conversion of the machine model from the abc reference frame to the d-q rotating reference frame model. The d-q model of an induction machine can be obtained by applying Park's transformation equation to the abc reference frame model [46]. The d-q equivalent circuit of a SEIG is shown in Fig. 1 [31].

The instantaneous voltages and currents of the SEIG can be presented at instant KT_s as following:

$$u_{ds} = R_s i_{ds} + \frac{d\Psi_{ds}}{dt} - \omega_e \Psi_{qs} \quad (1)$$

$$u_{qs} = R_s i_{qs} + \frac{d\Psi_{qs}}{dt} + \omega_e \Psi_{ds} \quad (2)$$

$$0 = R_r i_{dr} + \frac{d\Psi_{dr}}{dt} - (\omega_e - \omega)\,\Psi_{qr} \tag{3}$$

$$0 = R_r i_{qr} + \frac{d\Psi_{qr}}{dt} + (\omega_e - \omega)\,\Psi_{dr} \tag{4}$$

Meanwhile, the mechanical dynamic is represented by

$$\frac{d\omega}{dt} = \frac{P}{J}(T_m - T_e) \tag{5}$$

where T_m and T_e are the input mechanical and developed electrical torques, respectively.

The d-q components of stator and rotor fluxes relate their relevant currents by the following expressions:

$$\Psi_{ds} = L_S i_{ds} + L_m i_{dr} \tag{6}$$

$$\Psi_{qs} = L_S i_{qs} + L_m i_{qr} \tag{7}$$

$$\Psi_{dr} = L_m i_{ds} + L_r i_{dr} \tag{8}$$

$$\Psi_{qr} = L_m i_{qs} + L_r i_{qr} \tag{9}$$

where:

$$L_s = L_{lS} + L_m \tag{10}$$

$$L_r = L_{lr} + L_m \tag{11}$$

Substituting Equation (6) to (9) into Equation (1) to (4), we obtain the state model of the SEIG in the (d-q) rotating frame of reference related to the stator as [37], [39]:

$$\frac{di_{ds}}{dt} = \frac{1}{\Upsilon 4}(L_r u_{ds} - L_r R_s i_{ds} + R_r L_m i_{dr} + (\omega_e L_s L_r - L_m^2 \omega_s) i_{qs} + (\omega_e L_m L_r - L_m L_r \omega_s) i_{qr}) \tag{12}$$

$$\frac{di_{qs}}{dt} = \frac{1}{\Upsilon 4}(L_r u_{qs} - L_r R_s i_{qs} + R_r L_m i_{qr} + (L_m^2 \omega_s - \omega_e L_s L_r) i_{ds} + (\omega_s L_m L_r - L_m L_r \omega_e) i_{dr}) \tag{13}$$

$$\frac{di_{dr}}{dt} = \frac{1}{\Upsilon 4}(-L_m u_{ds} - L_s R_r i_{dr} + R_s L_m i_{ds} + (\omega_s L_s L_r - L_m^2 \omega_e) i_{qr} + (\omega_s L_m L_s - L_m L_s \omega_e) i_{qr}) \tag{14}$$

$$\frac{di_{qr}}{dt} = \frac{1}{\Upsilon 4}(-L_m u_{qs} - L_s R_r i_{qr} + R_s L_m i_{qs} + (L_m^2 \omega_e - \omega_s L_s L_r) 4 i_{dr} + (\omega_e L_m L_s - L_m L_s \omega_s) i_{ds}) \tag{15}$$

with:

$$\Upsilon 4 = L_s L_r - L_m^2 \tag{16}$$

In these equations, (R_r, R_s) are the rotor and stator resistances per phase respectively, (L_r, L_s) are the rotor and stator inductances per phase, (L_{ls}, L_{lr}) are the stator and rotor leakage inductances per phase, (L_m) is the mutual inductance, (i_{ds}, i_{qs}) are the stator currents in the two-phase d-q reference frame, (i_{dr}, i_{qr}) are the rotor currents in the two-phase d-q reference frame, (ω) is the electrical angular rotor frequency; $(\omega = p\omega_m)$; p is the number of pairs of poles, (ω_m) is the mechanical angular rotor frequency, (ω_e) is the synchronous speed, and $\omega_s = (\omega_e - \omega)$ is the slip speed.

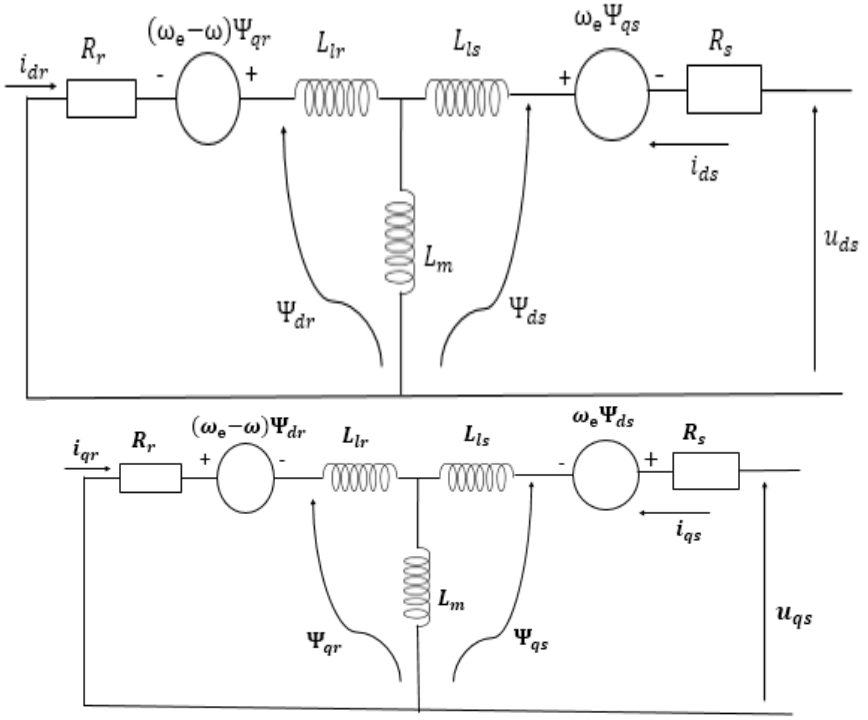

Fig. 1. D-q model of 3-phase induction generator

2.2. Overall Layout and Grid Modeling

As illustrated in Fig. 2, the direct driven SEIG is connected to the grid via two back-to-back power converters, and therefore an output filter must be utilized to handle the generated power to the grid. The filter takes the output of grid side converter (GSC) which is controlled to regulate the DC link voltage and achieve a unity PF operation, and then it provides the filtered quantities to the grid. Fig. 2 shows an illustration to this connection.

A Back-to-Back Power Converter [24] is a conFig.uration commonly used in (SEIG) systems to enable bidirectional power flow between the generator and the grid. It consists of two power converters, typically Voltage Source Converters (VSCs), connected back-to-back through a DC link. The back-to-back converter allows control of active and reactive power exchange between the SEIG and the grid, enhancing the system's stability, power quality, and grid integration capabilities.

Here's how the back-to-back power converter operates in an SEIG system:

- **Grid-Side Converter (GSC):** The first converter in the back-to-back conFig.uration, referred to as the grid-side converter, is connected to the electrical grid. Its primary function is to control the power flow between the SEIG and the grid. It can regulate the voltage and frequency of the power injected into the grid.
- **Machine-Side Converter (MSC):** The second converter, known as the generator-side converter, is connected to the SEIG's rotor. It enables the control of the generator's excitation and reactive power output. The converter adjusts the excitation current to maintain the generator's terminal voltage within the desired range and control the reactive power flow.
- **DC Link:** The GSC and RSC are connected through a DC link, which serves as the interface for power exchange between the two converters. The DC link capacitor smooth's out the voltage and helps maintain a stable DC voltage level.
- **Control Strategy:** The back-to-back power converter system requires a sophisticated control strategy to regulate the power flow between the SEIG and the grid. The control algorithms

calculate the required converter switching states based on voltage and current measurements, ensuring proper synchronization, pf control, and voltage stability.

The back-to-back power converter conFig.uration offers several benefits in SEIG systems:

1. **Grid Integration**: It enables the generator to supply power to the grid during excess generation or draw power from the grid during periods of low generation. This improves grid stability and facilitates renewable energy integration.
2. **Power Quality Enhancement**: It enables control of active and reactive power exchange, allowing for power factor correction and voltage regulation. It helps improve power quality by reducing voltage fluctuations, harmonics, and reactive power demand, ensuring a stable and clean power supply to the grid.
3. **Fault Ride-Through Capability:** It can enhance the SEIG's fault ride-through capability by providing dynamic support during grid faults or disturbances. It can rapidly control the generator's output and maintain voltage stability, allowing the SEIG to withstand and recover from grid faults.
4. **Control Flexibility**: The back-to-back power converter conFig.uration provides flexibility in controlling the SEIG system. By independently controlling the GSC and MSC, the system can adapt to varying grid conditions, load variations, and system requirements. It allows for dynamic adjustment of active and reactive power flow, voltage regulation, and grid support functions.

In summary, the back-to-back power converter conFig.uration is widely used in SEIG systems to enable efficient and reliable integration of the generator with the grid. It offers control flexibility, power quality enhancement, and improved grid stability, making it a valuable solution for renewable energy applications and distributed generation systems.

In a Self-Excited Induction Generator (SEIG), an RL (Resistor-Inductor) output filter is commonly employed to mitigate harmonics, reduce voltage distortion, and improve the quality of the generator's output voltage. The RL filter is connected between the output of the generator and the load, and it consists of a series combination of a resistor and an inductor.

The main functions and benefits of using an RL output filter in an SEIG are as follows:

- **Harmonic Filtering:** The SEIG inherently produces harmonics in its output voltage due to non-linear characteristics. The RL output filter helps suppress these harmonics by creating a low-impedance path for the high-frequency components. The inductor presents a high impedance to the harmonics, diverting them away from the load and reducing their impact on the connected devices.
- **Voltage Distortion Reduction:** The RL filter also helps in reducing voltage distortion caused by the SEIG's inherent voltage waveform imperfections. It smoothed out voltage irregularities and fluctuations, resulting in a more stable and sinusoidal output voltage waveform. This is particularly important when sensitive loads, such as electronic equipment or precision machinery, are connected to the SEIG.
- **Reactive Power Compensation:** The inductor component of the RL filter provides reactive power compensation to the SEIG system. The inductor absorbs and supplies reactive power, helping to balance the system's reactive power requirements and improve power factor correction. This contributes to overall system efficiency and reduces the burden on the SEIG.
- **Voltage Regulation:** The RL output filter can help improve voltage regulation by maintaining a more stable output voltage under varying load conditions. The inductor component helps to smooth out voltage variations caused by load changes, providing a more consistent voltage level to the connected load.

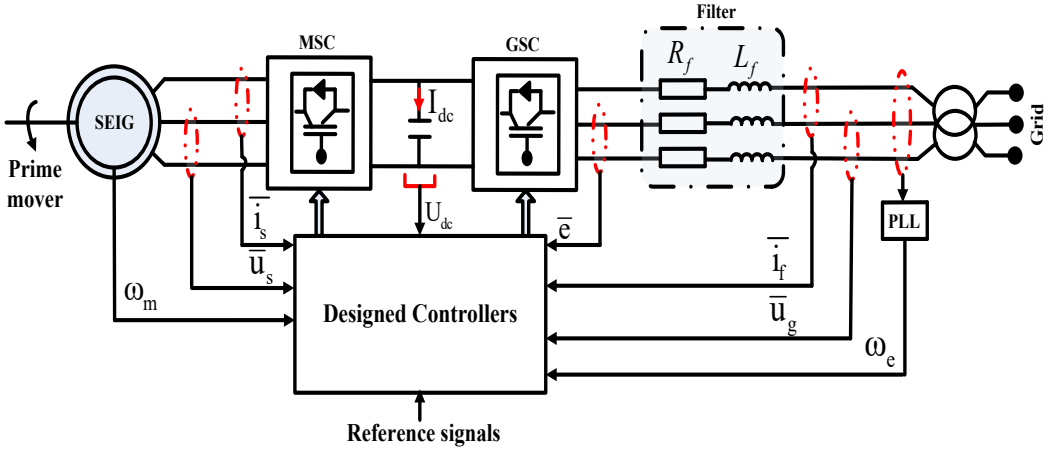

Fig. 2. Schematic diagram of direct driven grid connected SEIG

Considering that the grid voltage $\bar{u}_{g,k}$ is oriented to the q-axis of the rotating frame, then

$$u_{qg,k} = |\bar{u}_{g,k}| \; and \; u_{dg,k} = 0.0 \tag{17}$$

Then, the voltage balance across the filter is expressed by

$$\frac{di_{df,k}}{dt} = \frac{1}{L_f}\left(e_{d,k} - R_f i_{df,k} + \omega_{e,k} L_f i_{qf,k}\right) \tag{18}$$

$$\frac{di_{qf,k}}{dt} = \frac{1}{L_f}\left(e_{q,k} - R_f i_{qf,k} - \omega_{g,k} L_f i_{df,k} - u_{qg,k}\right) \tag{19}$$

where R_f and L_f are the grid filter's resistance and inductance. e_d and e_q are the GSC d-q voltages, ω_g is the angular frequency of the grid which is identified using a phase locked loop system [43]. Finally, i_{df} and i_{qf} are the d-q components of the filter current.

2.3. Converter's Modeling

A two-level three phase VSC model is utilized to represent the model of the generator and grid side converters. The VSI has 2^3 switching combinations, which provides eight possible voltages. The structure of the inverter and the voltages space representation are shown in Fig. 3.

The possible switching actions of any of the two converters can be mathematically represented using a single function as follows [40].

$$S = \frac{2}{3}(S_1 + \alpha S_2 + \alpha^2 S_3) \tag{20}$$

where $e^{j\frac{2\pi}{3}}$, and $S_{i,1,2,3}$ and $\bar{S}_{i,1,2,3}$ represent the on and off switching actions of the upper and lower switches and they equal $\{1,0\}$ and $\{0,1\}$, respectively.

Using the switching state S obtained from the controllers of generator and grid side converters, then the modulated generator and grid voltages can be calculated in terms of the DC link voltage and their corresponding switching states.

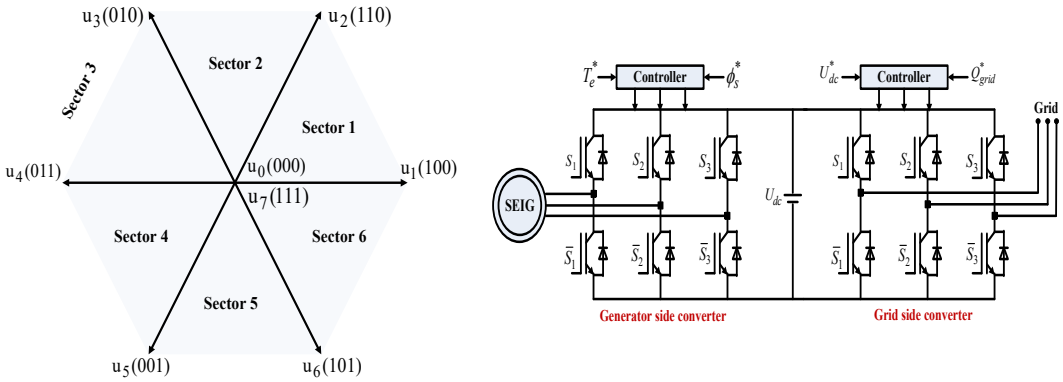

Fig. 3. (a) Voltage's representation space and (b) structure of the generator and grid side converters

3. Control Techniques of SEIG

The control system design for the wind energy conversion system's grid connection is shown in this section. While, the MSC's operation is governed by the predictive controllers (MPCC, MPDTC and designed PVC), the MPCC control is considered to control the GSC converter. Meanwhile, when the FOC is considered to regulate the MSC, the FOC is also considered to control the GSC converter.

3.1. Control Technique for Grid Side Converter

As stated earlier, the MPCC control topology is utilized to regulate the operation of GSC while considering the MPCC, MPDTC and proposed PVC for controlling the MSC converter. Control is achieved by a cost function form, which combines the absolute errors between the reference and predicted values of d-q filtered grid currents ($i_{df,k+1}, i_{qf,k+1}$) Thus, the cost function can be represented at instant $T_{s,k+1}$ by

$$\Delta i_{K+1} = \left| i^*_{df,k+1} - i_{df,k+1} \right|^i + \left| i^*_{qf,k+1} - i_{qf,k+1} \right| \quad (21)$$

where $i_{df,k+1}$ and $i_{qf,k+1}$ are the predicted values of filtered grid currents, which can be obtained as follows:

$$i_{df,k+1} = i_{df,k} + \left(\frac{di_{df,k}}{dt}\right) T_s \quad (22)$$

$$i_{qf,k+1} = i_{qf,k} + \left(\frac{di_{qf,k}}{dt}\right) T_s \quad (23)$$

where the two components $\left(\frac{di_{df,k}}{dt}\right)$ and $\left(\frac{di_{qf,k}}{dt}\right)$ can be obtained from equations (18) and (19).

According to the grid scheme in Fig. 4, grid voltage orientation along the q-axis of the rotating frame allows for the determination of the reference current ($i^*_{qf,k+1}$) by controlling the difference between the reference and actual DC link voltage values, while the d-axis reference current($i^*_{df,k+1}$) can be obtained as a function of the reference reactive power ($Q^*_{g,k+1}$), which is set to zero to achieve unity pf operation.

Fig. 5 presents a flow chart to display the operation steps of the MPCC for the grid-side converter which starts with estimating both the field current and grid voltage values and then sampling and holding. after that, the values of the d-q reference field current are calculated, and also compute the prediction values of the d-q field current through equation (22) and (23) ending with cost function determination to apply the voltage that gives the minimum value of it.

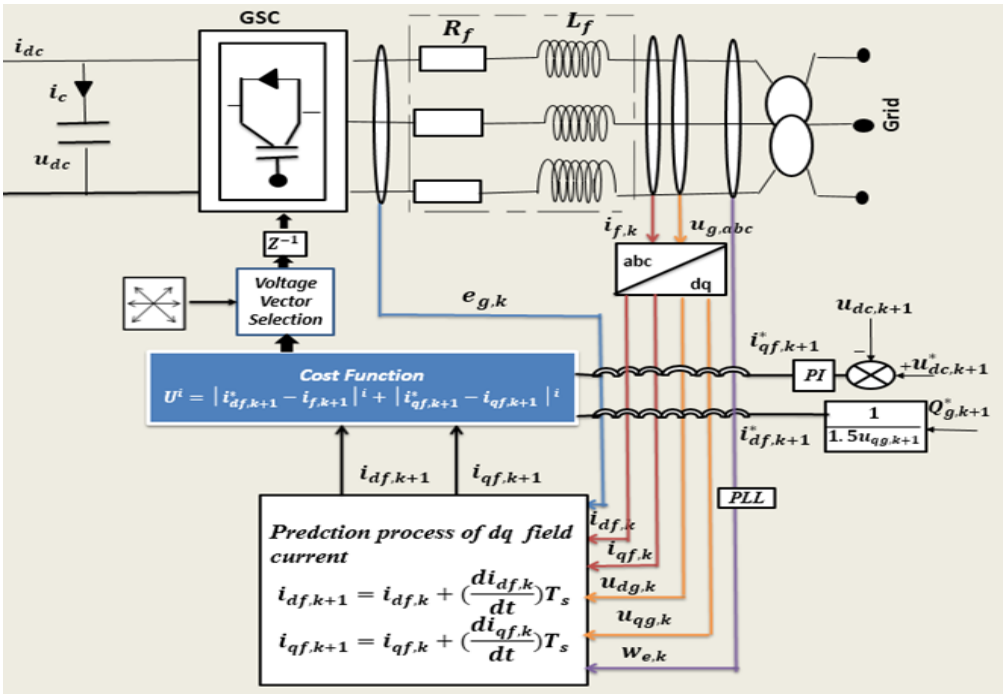

Fig. 4. MPCC for the grid-side converter

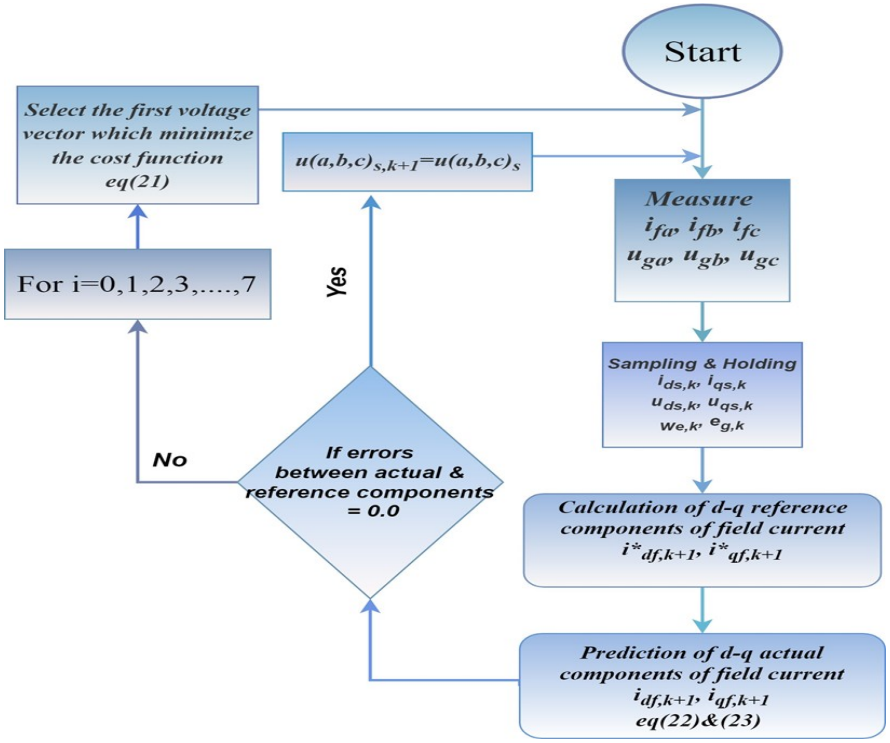

Fig. 5. Flow chart of MPCC for the GSC converter

3.2. Control Technique for Generator Side Converter

3.2.1. FOC Technique

Field-Oriented Control (FOC) is an independently controlled technology that modifies the torque and flux of the generator by aligning the rotor magnetic field with a revolving reference frame. This regulates the generator's output voltage and current. As part of the FOC technique, proportional integral (PI) controllers are frequently used to precisely control the rotor current of

SEIG, providing exact regulation of voltage and reactive power. The PI controllers are utilized in the following crucial control system components in FOC for SEIG:

1. Current control loop: In this loop, the PI controller's main job is to control the SEIG's stator current. The controller makes a comparison between the actual current and command current. The latter is usually derived from the voltage and power set points. The PI controller processes the difference between the reference and real current, and then produces a control signal to modify the (MSC) output voltage and regulate the excitation of the generator.
2. The voltage control loop is in charge of controlling the SEIG's output voltage. To keep the required voltage level in this loop constant, a PI controller is frequently used. The controller creates a control signal to modify the (GSC) output voltage so that it follows the intended set point after comparing the reference voltage and the actual output voltage.

The purpose of the PI controllers in FOC is to give the SEIG system precise and reliable control. While the Integral (I) component of the controller aids in the elimination of steady-state faults and enhances system stability, the Proportional (P) component aids in the prompt response to the error. The capacity of FOC to precisely control the output voltage, frequency, and power factor of the SEIG makes it relevant for controlling the SEIG. FOC can manage the excitation of the SEIG and enable steady and effective power generation. It is worth noting that while we are controlling the MSC under the FOC, also the GSC is controlled using the FOC principle.

3.2.1.1. Adaptive Control Strategy Design

In this subsection, the PI regulators for controlling the rotor flux, rotor speed, and q-axis current component as well as the PI regulator for controlling the DC-link voltage are derived as [14].

1. Design of Rotor Flux PI Regulator

The open-loop transfer function (OLTF) of the subsystem is given by

$$G_{\Psi_r}(s) = \frac{\Psi(s)}{i_{ds}(s)} = \frac{\frac{L_m R_r}{l_r}}{s + \frac{R_r}{L_r}} \tag{24}$$

where s is the Laplace operator

To control the rotor flux, two PI regulators are necessary. While the second regulator is used to regulate the stator current component $i_{ds,}$ the first regulator gives the reference stator current component i_{ds}^{*} . Let's use $e_{\Psi_r} = \Psi_r^* - \Psi_r$ and $C_{phi_r}(s)$ to represent, respectively, the tracking error and transfer function of the first PI regulator. The formula for $C_{\Psi_r}(s)$ is:

$$C_{\Psi_r}(s) = \frac{K_{P\Psi_r}(\frac{K_{i\Psi_r}}{K_{P\Psi_r}} + S)}{S} \tag{25}$$

The open-loop transfer function taking into account the PI regulator is

$$G_{OC_{\Psi_r}}(s) = \frac{K_{P\Psi_r} L_m R_r}{L_r} \text{ x } \frac{\frac{K_{i\Psi_r}}{K_{P\Psi_r}} + S}{S(S + \frac{R_r}{L_r})} \tag{26}$$

The compensation of the pole of $G_{OC_{\Psi_r}}(s)$ by the zero of the PI regulators yields

$$\frac{K_{i\Psi_r}}{K_{P\Psi_r}} = \frac{R_r}{L_r} \tag{27}$$

and

$$G_{OC_{\Psi_r}}(s) = \frac{L_m K_{P\Psi_r} R_r}{L_r S} \tag{28}$$

The closed – loop transfer function can be computed as

$$F_{\Psi_r}(s) = \frac{1}{L_r S \frac{L_r}{R_r L_m K_{P\Psi_r}} S + 1} \tag{29}$$

The above closed – loop transfer function represents a standard first order system with time constant of $\tau_{\Psi_r} = \frac{L_r}{R_r L_m K_{P\Psi_r}}$.

The first-order unit step response is generally known to be within 95% of its steady-state value after three time constants. So, in the case of a first-order system, the settling time $t_{s(5\%)}$, which is commonly defined as the period at which the response enters and stays within a ±5% band about the steady-state value, can be approximated by:

$$t_{S_{\Psi_{r(5\%)}}} = 3\tau_{\Psi_r} \tag{30}$$

Consequently, given a desired settling time$t_{S_{\Psi_{r(5\%)}}}$, from (27) and (30), we can deduce the expressions for $K_{P\Psi_r}$ and $K_{i\Psi_r}$ as

$$K_{P\Psi_r} = \frac{3L_r}{R_r L_m t_{\Psi_r(5\%)}} \tag{31}$$

$$K_{i\Psi_r} = \frac{3}{L_m t_{S\Psi_r(5\%)}} \tag{32}$$

2. Stator Current Components i_{ds} and i_{qs} Regulation

$$u_{ds} = R_s i_{ds} + \frac{d\Psi_{ds}}{dt} - \omega_e \Psi_{qs} \tag{33}$$

$$u_{qs} = R_s i_{qs} + \frac{d\Psi_{qs}}{dt} + \omega_e \Psi_{ds} \tag{34}$$

The existence of coupling terms between the d- and q-axes may be seen from (33) and (34). A decoupling circuit is added to the outputs of the PI regulators to limit the effects of one input on only one output and thereby dissipate the coupling between the two axes (see Fig. 5).

The following definitions of new control variables are necessary due to the operational principle of this circuit:

$$v{u_{ds}}^{dec} = \frac{di_{ds}}{dt} + \Upsilon 1 i_{ds} \tag{35}$$

$$v{u_{qs}}^{dec} = \frac{di_{qs}}{dt} + \Upsilon 1 i_{qs} \tag{36}$$

Remark 1. Since ${u_{ds}}^{dec}$ and ${u_{qs}}^{dec}$ from (35) and (36) are in charge of controlling the direct axis stator current i_{ds} and quadrature axis component i_{qs} respectively, the control goals can now be seen as a decoupling problem. Now that the transfer functions from (35) and (36) have been determined as (37) and (38).

$$\frac{i_{ds}}{u_{ds}{}^{dec}} = \frac{\upsilon}{s+\gamma 1} \tag{37}$$

$$\frac{i_{qs}}{u_{qs}{}^{dec}} = \frac{\upsilon}{s+\gamma 1} \tag{38}$$

As in the case of Ψ_r, it is simple to compute the equations for the PI regulators of $i_{ds}\ and\ i_{qs}$ control as follows:

$$K_{pi_{ds}} = \frac{3}{\upsilon t_{Si_{ds}}}, K_{ii_{ds}} = \frac{3\gamma 1}{\upsilon t_{Si_{ds}}} \tag{39}$$

$$K_{pi_{qs}} = \frac{3}{\upsilon t_{Si_{qs}}}, K_{ii_{qs}} = \frac{3\gamma 1}{\upsilon t_{Si_{qs}}} \tag{40}$$

Remark 2. Take note that the above-mentioned PI regulators cannot be used in practice because their parameters, rotor flux and rotor resistance, are not online measurably [32]. Additionally, the rotor resistance a time-varying unknown parameter determines the rotor flux and the stator electrical angular position. Consequently, in order to implement the above controllers practically, an online adaptation law for R_r and observer for Ψ_r are needed.

However, the complexity resulting from the use of the coordination transformation, it involves multiple control loops, and its reliance on the machine parameters as a result of the PI are still major drawbacks of the FOC. So, we use other control techniques to overcome these drawbacks as shown in the Fig. 6.

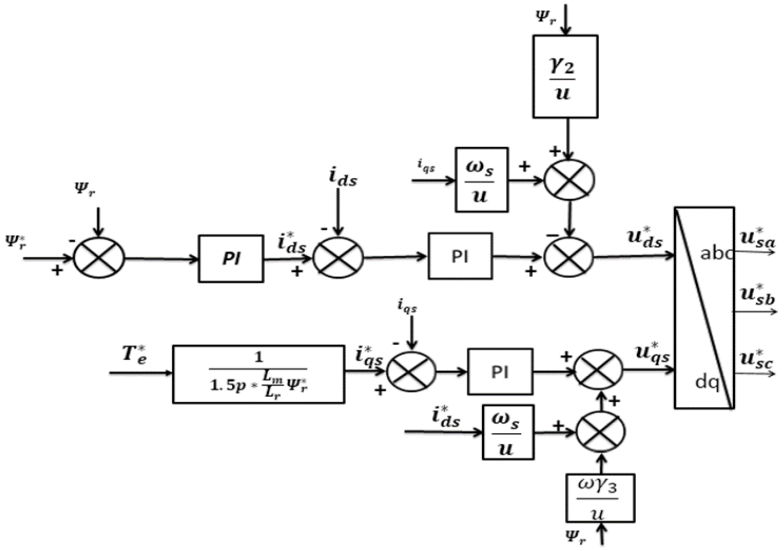

Fig. 6. FOC scheme for generator side converter

3.2.2. MPCC Technique

MPCC is a control strategy that utilizes a predictive model does not require a weighting factor (ω_f) because it uses a simple cost function made up of two comparable terms, the errors between the actual and reference values of the stator current. Taylor expansion can be used to predicted the actual stator current components $i_{ds,(k+1)}$ and $i_{qs,(k+1)}$, While stator current reference values $i^*_{ds,k+1}$ and $i^*_{qs,k+1}$, may be directly determined using the reference values of the active and reactive powers. According actual value of stator current components, the predictive can be evaluated as (41) and (42).

$$i_{ds,k+1} = i_{ds,k} + (\frac{di_{ds,k}}{dt})T_s \quad (41)$$

$$i_{qs,k+1} = i_{qs,k} + (\frac{di_{qs,k}}{dt})T_s \quad (42)$$

The derivatives of the stator current components at instant kT_s can be given by

$$\frac{di_{ds,k}}{dt} = \frac{1}{L_sL_r - L_m^2}(L_r u_{ds,k} - L_r R_s i_{ds,k} + R_r L_m i_{dr,k} + (\omega_e L_s L_r - L_m^2\omega_s)i_{qs,k}(\omega_e L_m L_r - L_r\omega_s)i_{qr,k}) \quad (43)$$

$$\frac{di_{qs,k}}{dt} = \frac{1}{L_sL_r - L_m^2}(L_r u_{qs,k} - L_r R_s i_{qs,k} + R_r L_m i_{qr,k} + (-\omega_e L_s L_r + L_m^2\omega_s)i_{ds,k}(-\omega_e L_m L_r + \omega_s)i_{dr,k}) \quad (44)$$

The reference values of the stator current at instant $(K+1)T_s$ can be calculated by:

$$i^*_{ds,k+1} = \frac{|\Psi^*_{r,k+1}|}{L_m} \quad (45)$$

The reference value of the quadrature axis component of stator current at instant $(K+1)T_s$ can be calculated in terms of the reference value of applied mechanical torque so

$$\Psi_{dr,k+1} \approx |\Psi_{r,k+1}| \quad where \quad \Psi_{qr,k+1} \approx 0.0$$
$$i^*_{qs,k+1} = \frac{T^*_{e,k+1}}{1.5p * \frac{Lm}{Lr} * |\Psi^*_{r,k+1}|} \quad (46)$$

Finally, the actual and reference stator current components are fed to the cost function, which can be expressed by the following.

$$U^i = \left| i^*_{ds,k+1} - i_{ds,k+1} \right|^i + \left| i^*_{qs,k+1} - i_{qs,k+1} \right|^i \quad (47)$$

Fig. 7 illustrates how the MPCC scheme can be built. It measures the stator voltage and current while estimating the rotor current and sampling the entire amount. After measuring the rotor speed at instant KT_s (ω_k) the rotor location $(\theta_{e,k})$ is found by integrating the data. The measured values were transformed into d-q components$(i_{ds,k}, i_{qs,k}, i_{dr,k}, i_{qr,k}, u_{ds,k}, u_{qs,k})$, and so on. Using the Taylor expansion($i_{ds,k+1}$,$i_{qs,k+1}$), the actual stator current values are anticipated. Using the reference active and reactive powers, the stator current reference values are computed.

Finally, the cost function in Equation (47) receives inputs from both the actual and reference anticipated values of the stator current. Next, the cost function is calculated by the system, which records its value continuously, finds its lowest value, applies it, and then indicates that it has completed its computation by applying the lowest value to the MSC.

Where the superscript ^{i} denotes the sectors (0 . . . 7). The cost function (47) represents the core of the MPCC, based upon which the optimal voltage vectors are selected.

Fig. 8 presents a flow chart to display the operation steps of the MPCC for the generator-side converter which starts with measure both the stator current and voltage, then sampling and holding them and rotor current. after that, the values of the d-q reference stator current are calculated using equation (45) and (46), then compute the prediction of the d-q actual values stator current through equation (41) and (42) ending with cost function determination to apply the voltage that gives the minimum value of it.

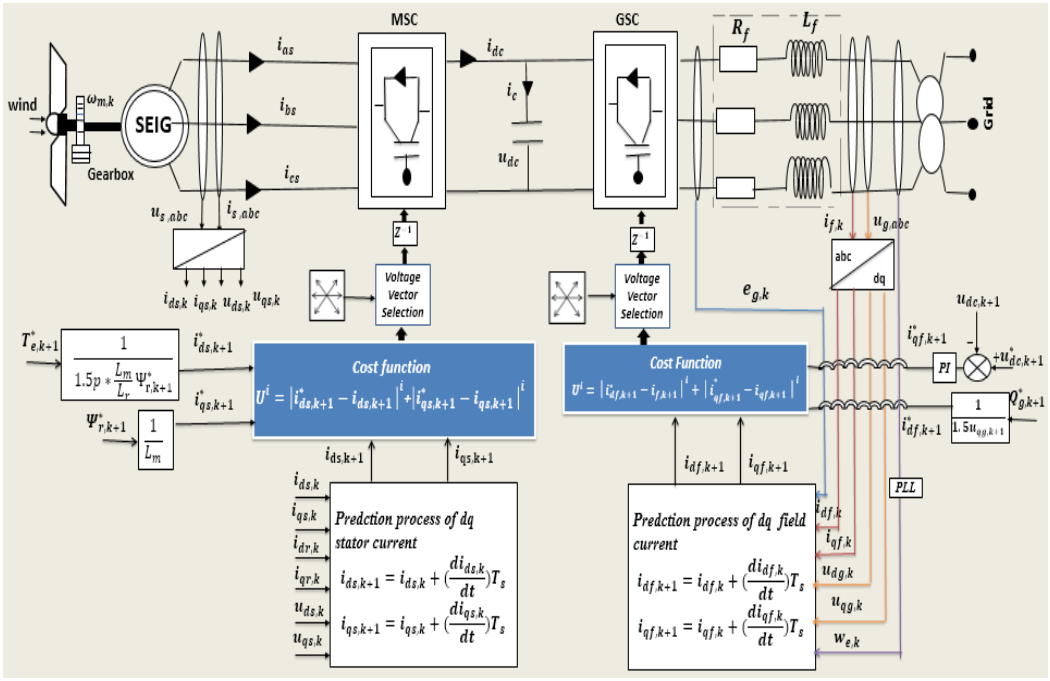

Fig. 7. MPCC technique for the SEIG

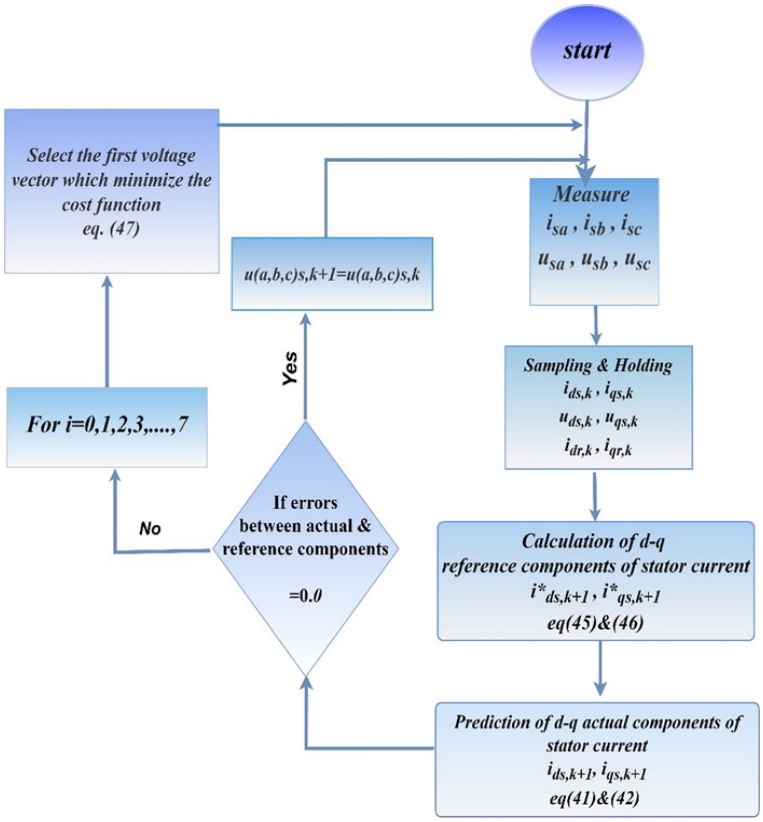

Fig. 8. Flow chart of MPPC for the grid-side converter

3.2.3. MPDTC Technique

MPDTC depends on regulating the torque and rotor flux, which can be accomplished by eliminating the difference between the reference and predicted actual torque signals (T^*_{k+1} and

T_{k+1}) and between the reference and predicted actual rotor flux signals ($\Psi^*_{r,k+1}$ and $\Psi_{r,k+1}$) the cost function can be expressed as (48).

$$A^i = \left| T^*_{e,k+1} - T_{e,k+1} \right|^i + w_f \left| \Psi^*_{r,k+1} - \Psi_{r,k+1} \right|^i \quad (48)$$

Equation (48) includes variables that need to be evaluated using the machine parameters, it also requires current calculation, which is used for estimating and predicting the torque and rotor flux, and all of this increases the computation time. Furthermore, the function needs a weighting factor ($w_f = \frac{T,nominal}{\Psi_{r,nominal}}$) [21] that is required for ensuring the equilibrium between the torque and rotor flux. If the weighting factor is inappropriately selected, the torque and rotor flux ripples are negatively affected there is a procedure which tried to choose the optimal weighting factor in an online manner, which reduced the deviations in the torque and rotor flux, but unfortunately, the computational burden was affected. Hence, the weighting factor is still a major obstacle to MPDTC. The reference value of rotor flux $\Psi^*_{r,k+1}$ is assigned to the rated value ($\Psi^*_{r,k+1} = 1$) and the reference torque is obtained from the output of a PI speed controller. The actual value of the rotor flux $\left| \Psi_{dr,k+1} \right|$ can be predicted and calculated at instant $(K+1)T_s$ in the following manner:

$$\left| \Psi_{r,k+1} \right| = \sqrt{(\Psi_{dr,k+1})^2 + (\Psi_{qr,k+1})^2} \quad (49)$$

where $\Psi_{dr,k+1}$ and $\Psi_{qr,k+1}$ can be formulated as follows:

$$\Psi_{dr,k+1} = L_r i_{dr,k+1} + L_m i_{ds,k+1} \quad (50)$$

$$\Psi_{qr,k+1} = L_r i_{qr,k+1} + L_m i_{qs,k+1} \quad (51)$$

where the stator current components $i_{ds,k+1}$ and $i_{qs,k+1}$can be predicted using Equations (41) and (42), and the rotor current components $i_{dr,k+1}$ and $i_{qr,k+1}$ can be predicted in the same manner. The actual predicted value of the torque $T_{e,k+1}$can be expressed by the following:

$$T_{e,k+1} = 1.5p\frac{L_m}{Lr}(\Psi_{dr,k+1} i_{qs,k+1} - \Psi_{qr,k+1} i_{ds,k+1}) \quad (52)$$

The scheme of MPDTC is illustrated in Fig. 9, in which the stator voltages, stator current are measured whereas rotor current is estimated and then sampled all. The rotor speed (ω_k) is measured and then integrated to find the rotor position ($\theta_{e,k}$). The actual values of the stator and rotor currents are predicted using Taylor expansion [47], [48], and these components are then used to calculate the actual values of the torque and rotor flux. The reference values of the stator and rotor currents are calculated using the reference active and reactive powers; after that, these components are used to compute the reference values of the torque and rotor flux.

Finally, the reference and actual predicted values of the torque and rotor flux are fed to the cost function in Equation (43). Fig. 10 presents a flow chart to display the operation steps of the MPTC, in which both stator voltages and stator current are measured then after that all these variables and rotor current are sampled, then the prediction values of the dq stator current and rotor current are computed according to equations (41) and (42) to utilize them to determine the prediction actual values of d-q rotor flux using equations (50) and (51), then used to predict actual values of torque and rotor flux according equations (49) and (52) in the same time the reference values of the rotor flux and torque are calculated through equations (46). In the last step, the cost function minimizes the errors in the reference and prediction values of the rotor and torque accordion to equation (48) to apply the voltage which achieves this minimization.

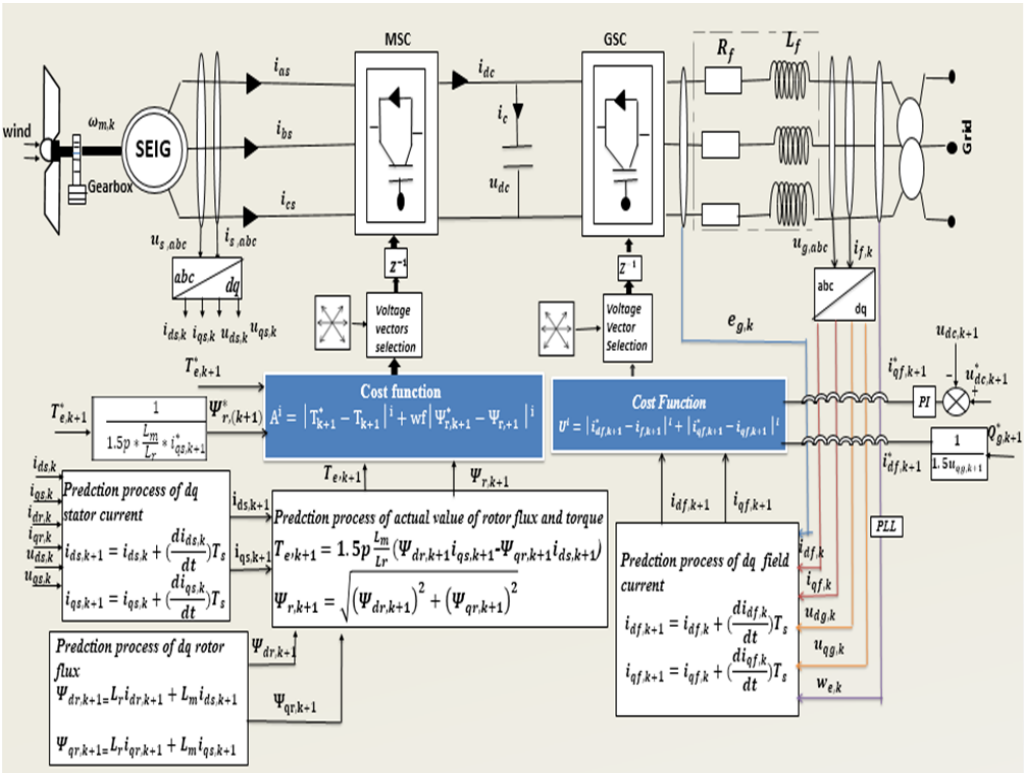

Fig. 9. MPDTC technique for the SEIG

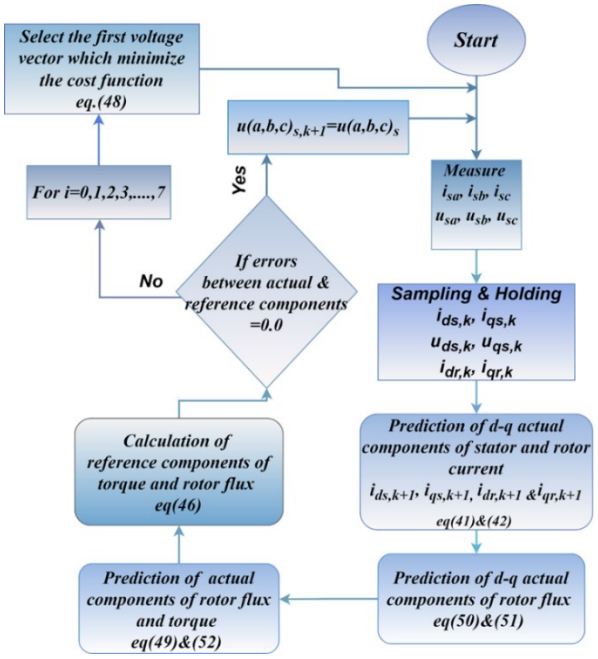

Fig. 10. Flow chart of MPDTC for the generator-side converter

3.2.4. Proposed PVC Technique

The proposed PVC (predictive voltage control) utilizes a very simple cost function that has two similar terms, which are the errors between the reference and actual values of the stator voltage. The adopted cost function can be expressed by (53).

$$C_i = \left|u^*_{ds,k+1} - u_{ds,k+1}\right|^i + \left|u^*_{qs,k+1} - u_{qs,k+1}\right|^i \quad (53)$$

Since the goal of the adopted cost function is to minimize the difference between the reference and predicted actual values of the d-q components of the generator's voltage, as can be seen from equation (53) and since its components are analogous, it does not need a weighting factor (w_f), which can lead to a mismatch issue as in the case of traditional predictive control schemes. The cost function is also devoid of estimated variables that are derived from the model parameters, which helps to address the problem of system uncertainties and make it resilient to changes in parameter values so these method overcame the shortages of previous predictive control methods like (MPCC, MPDTC) and also the shortages of field oriented control method (FOC).

The method shown in Fig. 11, explains how the suggested PVC can provide the stator voltages needed to match the required reference values. The major goal of this system is to reduce the difference between the reference and actual values of stator voltage. Fig. 8, displays the possible controller behaviors. As shown this Fig.ure, it is assumed that sector 6 contains the reference stator voltage vector ($\bar{u}_s^*$). the cost function (53) begins by determining which voltage vector can achieve the lowest error, or lowest departure from the reference value. Within sector 6, three bisectors (S1, S2, and S3) develop by cutting the sector's inter-median lines. We can see that there are three vectors that can occupy this position $u_1(100), u_6(101)$, and $u_0(000)$ or $u_7(111)$. However, the switching state $\{u_6(101)\}$ is the optimal vector because it yields the lowest deviation ($\bar{u}_{e1}$) value. As a result, the suggested PVC can apply (47) and track the location of the reference vector to achieve the control targets with a minimal computing overhead.

Now, the actual stator voltage $(u_{ds,k+1}$ and $u_{qs,k+1})$ can be obtained directly through the switching states of the voltage source inverter (VSI), using the finite control set (FCS) principle, which refers to a control strategy that utilizes a finite set of discrete control values or actions instead of using a PWM topology that using a continuous range of control signals, the FCS [26] operates with a predefined set of discrete control values. These control values are typically represented by binary codes or digital signals which simplify the control implementation, FCS control can offer fast response times because the discrete control actions can be rapidly switched.

As an alternative, the reference values for the stator voltage $(u^*_{ds,k+1}$ and $u^*_{qs,k+1})$ are produced by using the two PI current controllers that were previously constructed. The two PI current regulators' detailed designs and gain selections are provided in Sec (3.2.1). The reference voltage components are outputted by the PI regulators along with the divergence between the d-q current components ($i_{ds,k+1}$ and $i_{qs,k+1}$) and their references$(i^*_{ds,k+1}$ and $i^*_{qs,k+1})$. We can obtain the reference values of d-q stator voltages ($u^*_{ds,k+1}$ and $u^*_{qs,k+1}$) by using FOC technique as mentioned in sec (3.2.1) after being reformulated at instant $(k+1)T_s$. The complete PVC control system can be illustrated as shown in Fig. 12 while in.

Fig. 13 presents a flow chart to display the operation steps of the PVC, in which both stator voltages and stator current are measured then after that all these variables and rotor current are sampled, then the prediction values of the d-q stator current and rotor current are computed according to equations (41) and (42) to utilize them to determine the prediction of actual values of d-q rotor flux using equations (50) and (51), then used to predict actual values of torque and rotor flux according equations (49) and (52) in the same time the reference values of the rotor flux and torque are calculated through equations (46), then the d-q reference voltage are evaluated using PI controller. In the last step, the cost function minimizes the errors in the reference and prediction values of the stator voltage according to equation (53) to apply the voltage which achieves this minimization.

In brief, The proposed predictive voltage control provide several advantages such as it uses very simple cost function which consists of the absolute errors between the reference and actual values of stator voltage component help in reducing significantly the complication needed by the predictive controller because the actual voltage component needed by the cost function can be directly obtain from the switching signal of the inverter after adjusting the finite control set (FCS)

also the reference voltage component (u_{ds}^{*} and u_{qs}^{*}) can be obtained via reference way which has a flexibility for the control designer in designing the cost function so no of switching loss reduced in system, low ripple in any generated variables , low harmonics, and it is faster dynamic response, as its time response is less than the time response of the other control methods, as it is less than the response time of FOC by 15%, less than the response time of MPCC by 9% and less than the time response of MPDTC by 4%.so we get to desired performance of the generator as soon as possible This increases the efficiency and reliability of the system as it responds quickly to loads. And number of commutations is produced by PVC is less than the number of commutations for MPCC by 38% and by 40% for MPDTC.

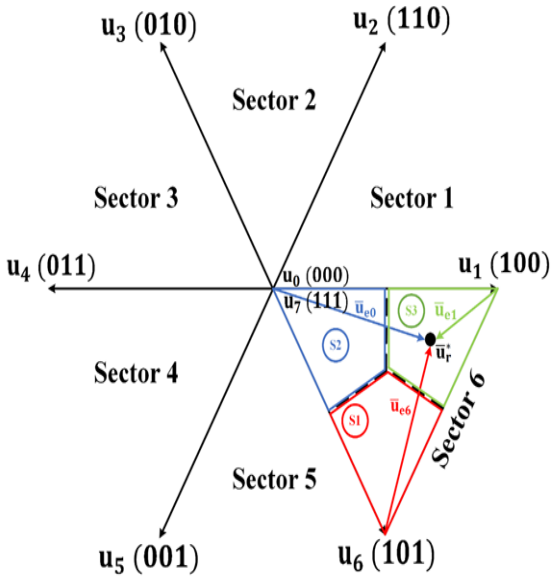

Fig. 11. Mechanism of selection the optimal stator voltage using PVC

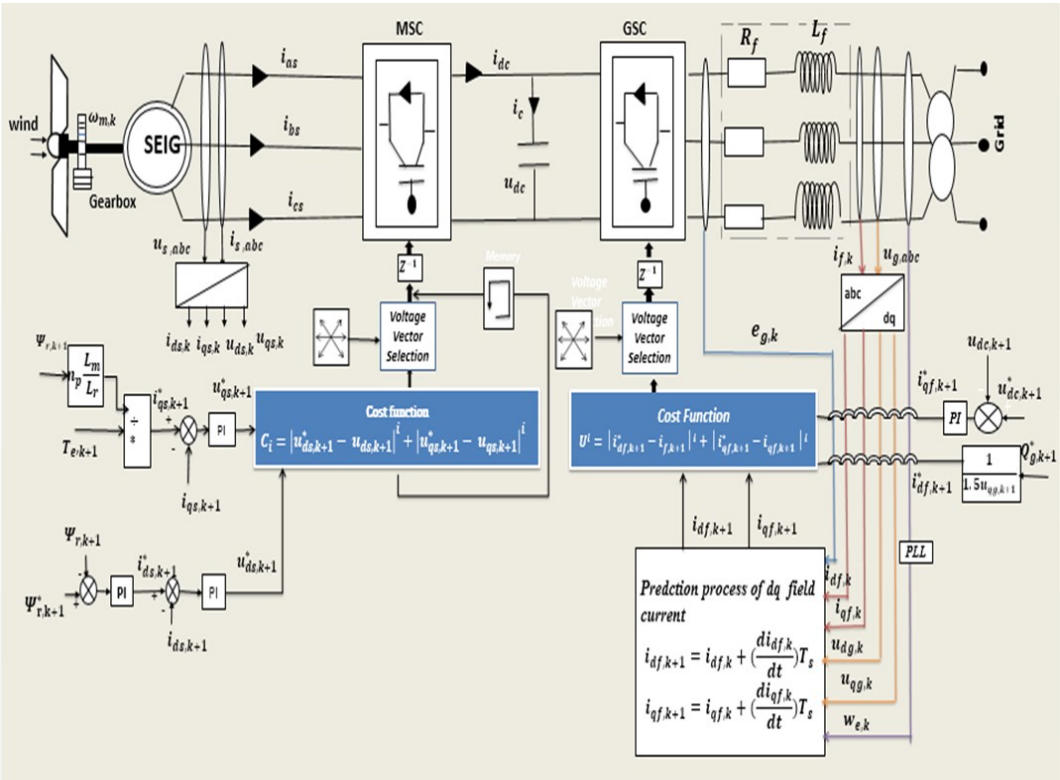

Fig. 12. Proposed PVC technique for the SEIG

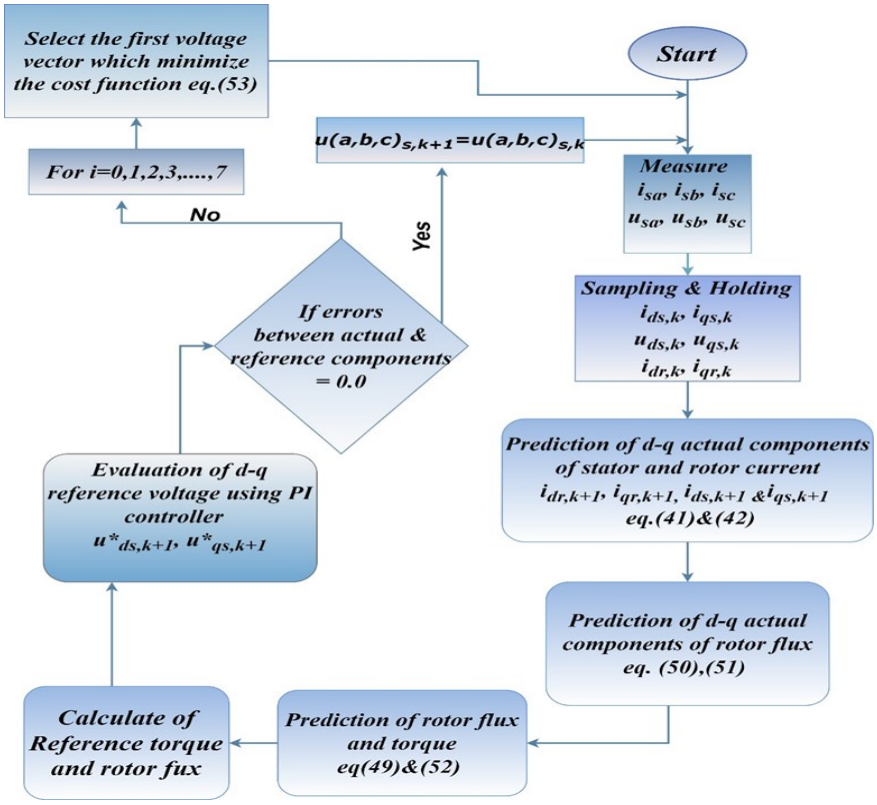

Fig. 13. Flowchart of PVC for the generator-side converter

4. Test Results

Tests were carried out using MATLAB simulation for the four control techniques (FOC, MPCC, MPDTC, and proposed PVC) under operating condition in which the generator is directly driven using a prime mover while changing the applied mechanical torque from 12 Nm to 20 Nm (rated torque).

4.1. Testing with FOC Technique

The SEIG's performance was tested with the FOC technique for the operating condition shown in Fig. 14. The results obtained for this condition, which are shown in Fig. 15 – Fig. 22 for the varying applied mechanical torque demonstrate that the active power, reactive power, developed torque, and rotor flux smoothly follow their reference values.

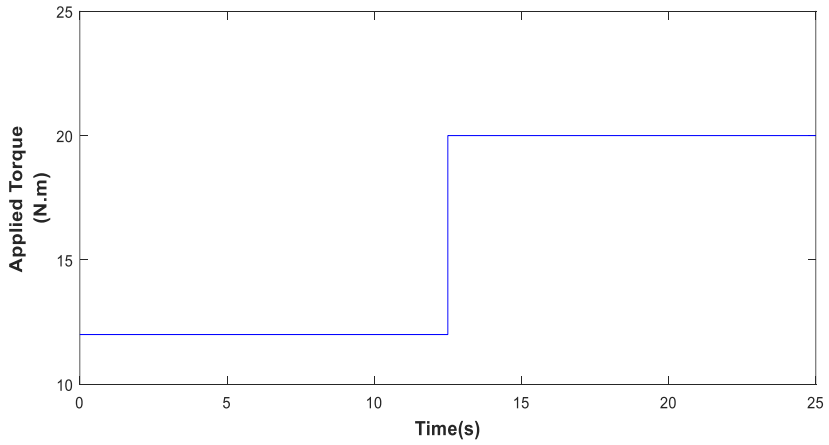

Fig. 14. Applied mechanical torque from prime mover (Nm)

In addition, the actual d-q stator currents in Fig. 21 and Fig. 22 follow their references with good tracking. It can be concluded that the FOC is ripple-free, and the estimated values of the powers, torque, and rotor flux are tracking their references in a good manner. It is also noted that a unity PF operation at grid side is ensured thanks to the adopted control of GSC. The reactive grid power Fig. 16 is maintained at zero value; meanwhile the active gird power Fig. 15 follows the variation in the applied mechanical torque on the generator's shaft. The main drawbacks are the control system complexity and the delayed dynamic response caused by the PI current regulators. Another noticeable drawback is the over and under shots in the estimated variables due to the dependency on the designed current and flux controllers.

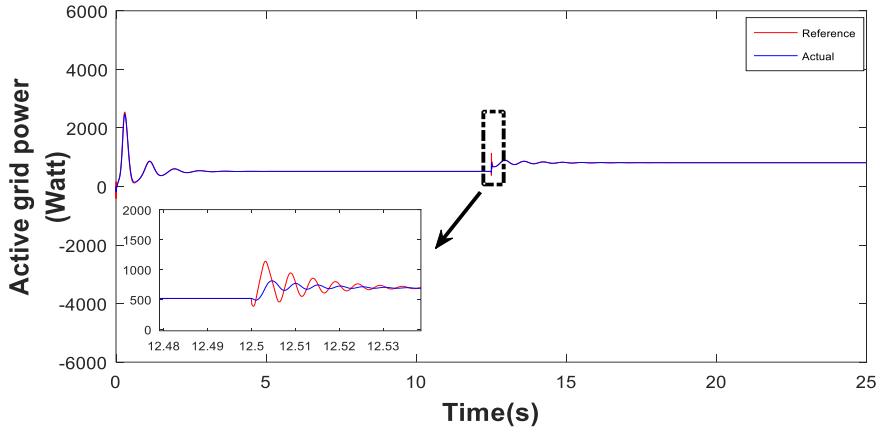

Fig. 15. Active grid power under FOC (Watt)

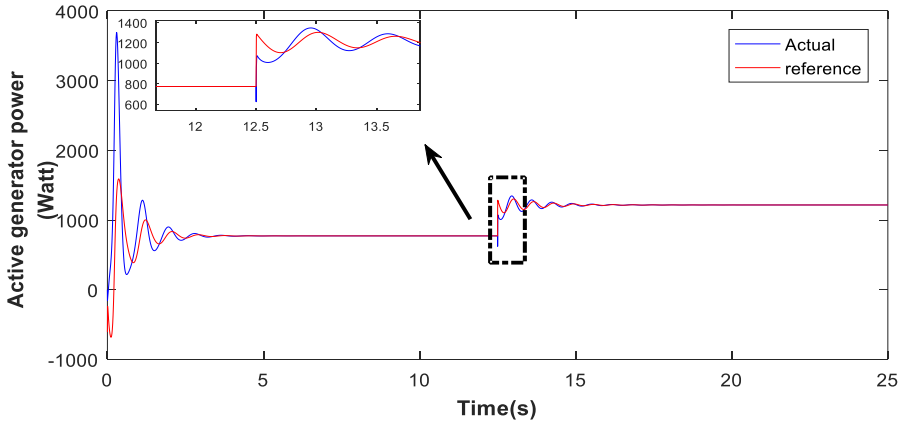

Fig. 16. Active generator power under FOC (Watt)

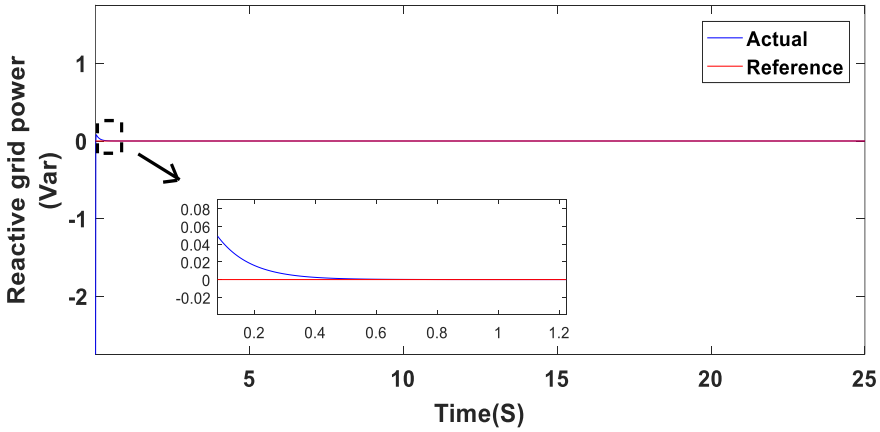

Fig. 17. Reactive grid power under FOC (Var)

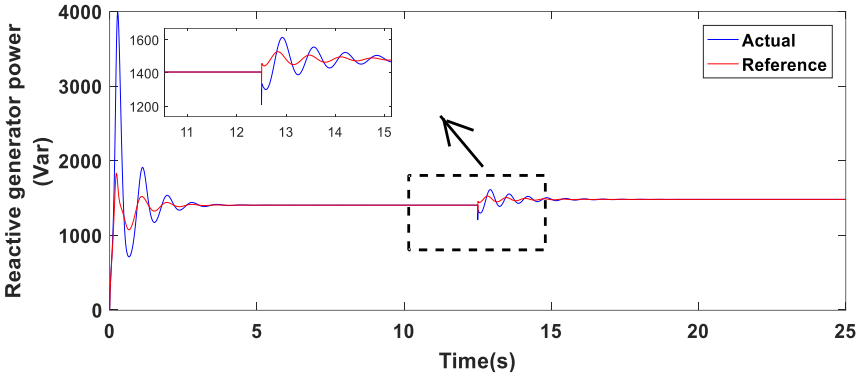

Fig. 18. Reactive generator power under FOC (Var)

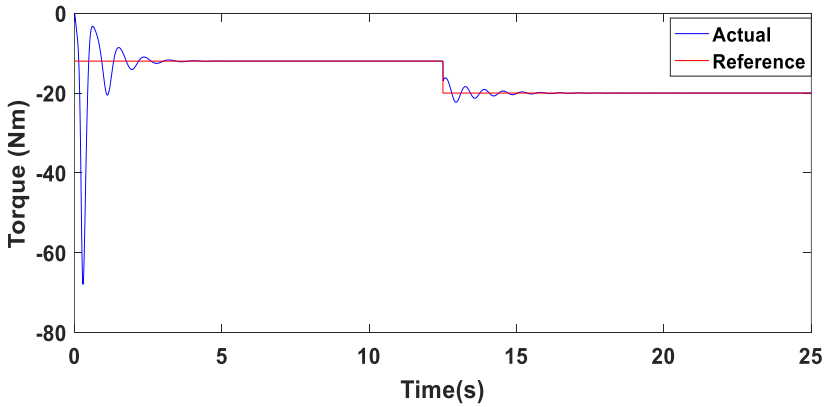

Fig. 19. Developed torque under FOC (Nm)

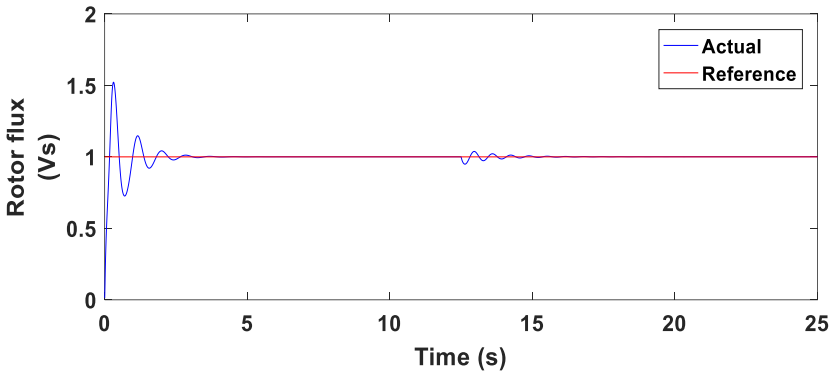

Fig. 20. Rotor flux under (FOC) (Vs)

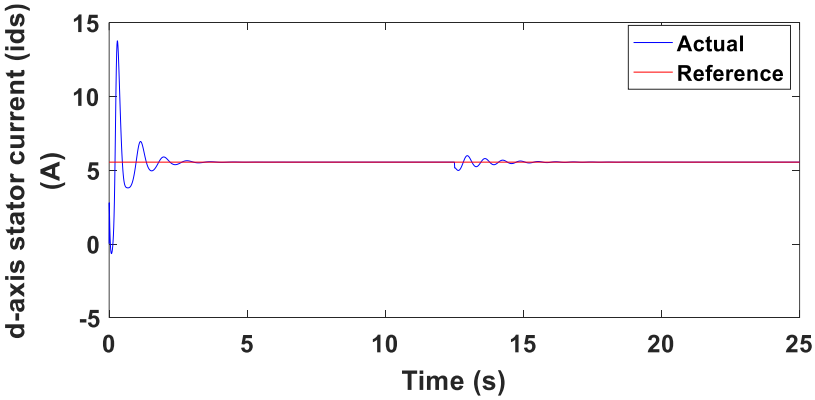

Fig. 21. d-axis stator current (i_{ds}) under (FOC) (A)

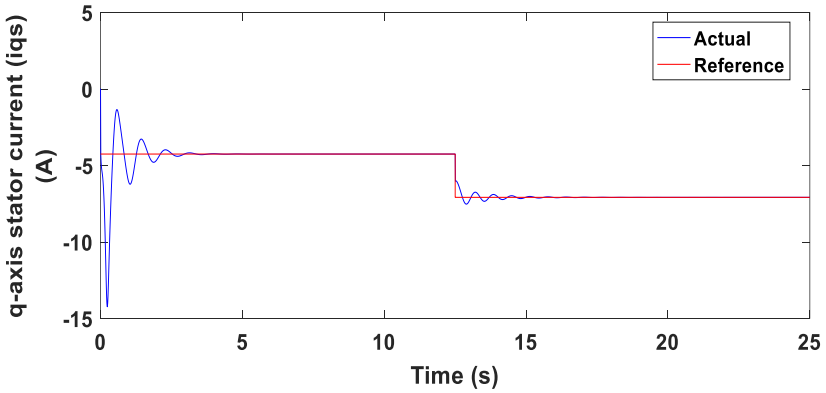

Fig. 22. q-axis stator current (i_{qs}) under (FOC)

4.2. Testing with MPCC Technique

The IG's performance was tested with the MPCC technique for the operating condition presented in Section 4.1. The obtained results show that, although its ripples are noticeable when compared to the FOC approach as it has low ripples because it does not contain (w_f), but they are still there as it depends on model parameters, the actual values of the active and reactive powers, torque, and rotor flux follow their references with a dynamic response faster than that of the FOC principle as the time response taken by active generator power in Fig. 23 to reach it's reference power of MPCC is faster than the time response taken by FOC by 5.7%. In Fig. 24 and Fig. 26 active and reactive grid power obtained at zero while active generator power in Fig. 25 followed the applied mechanical torque on the shaft and in Fig. 27 reactive generator power follow the magnetization of generator.

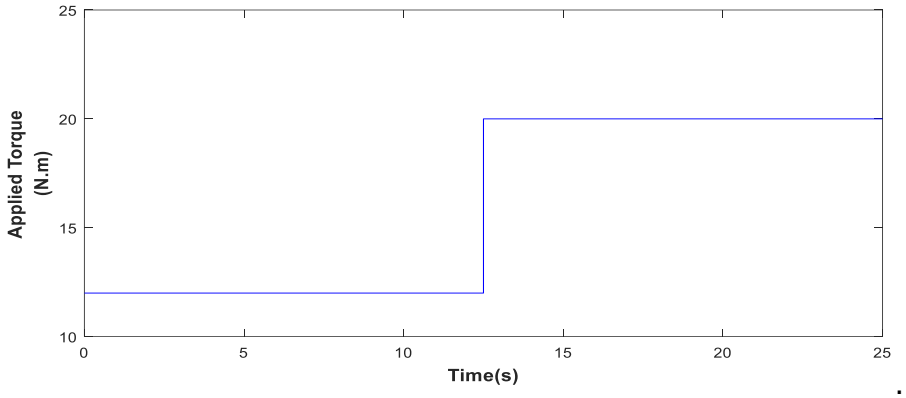

Fig. 23. Applied mechanical torque from prime mover (Nm)

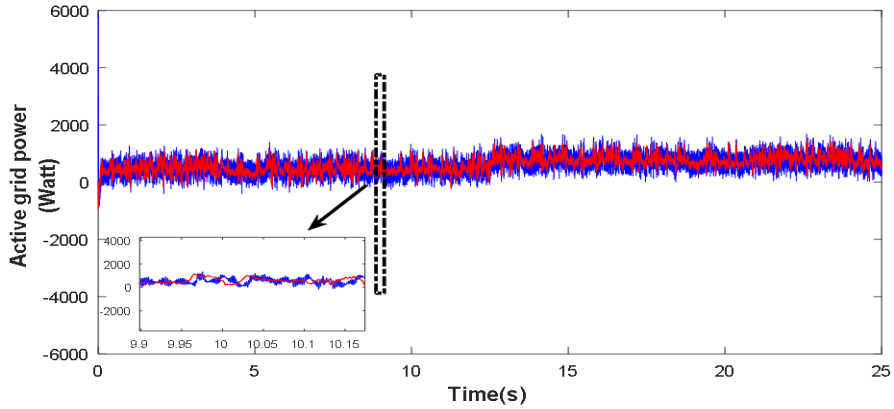

Fig. 24. Active grid power under MPCC (Watt)

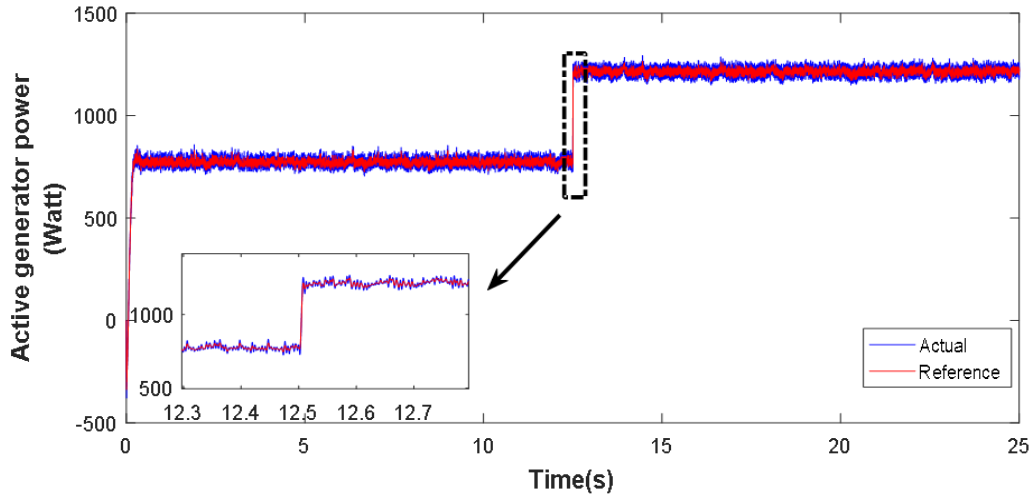

Fig. 25. Active generator power under MPCC (Watt)

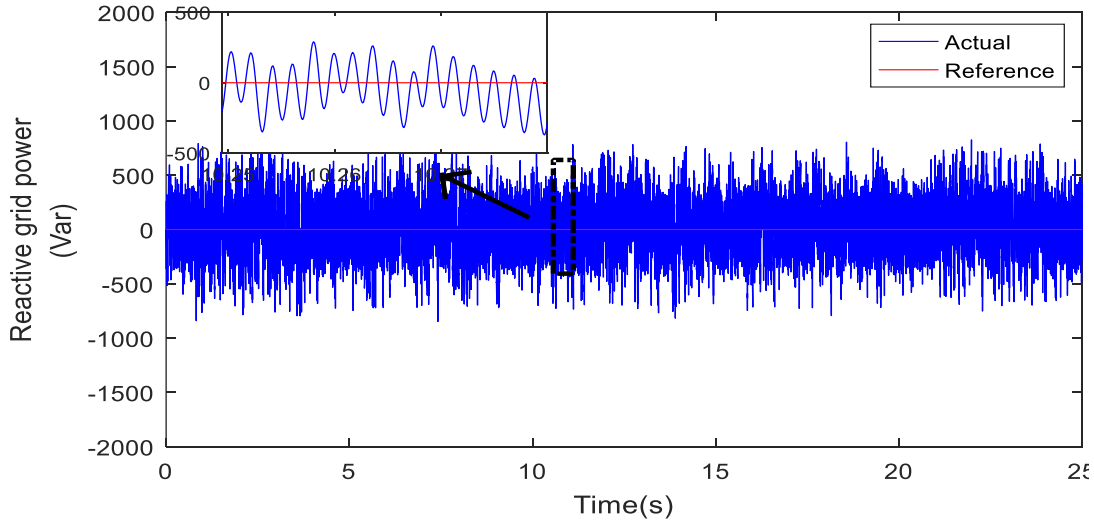

Fig. 26. Reactive grid power under MPCC (Var)

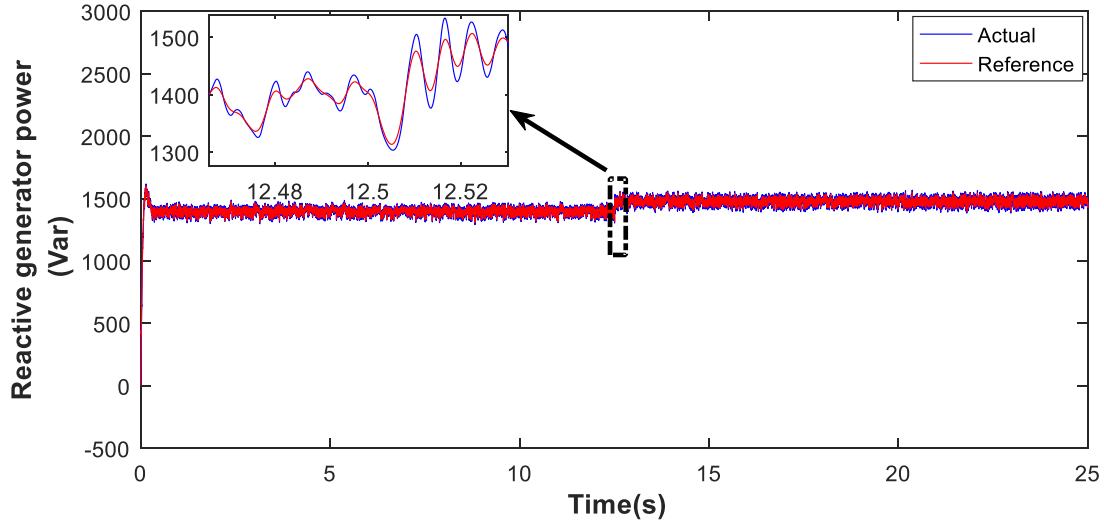

Fig. 27. Reactive generator power under MPCC (Var)

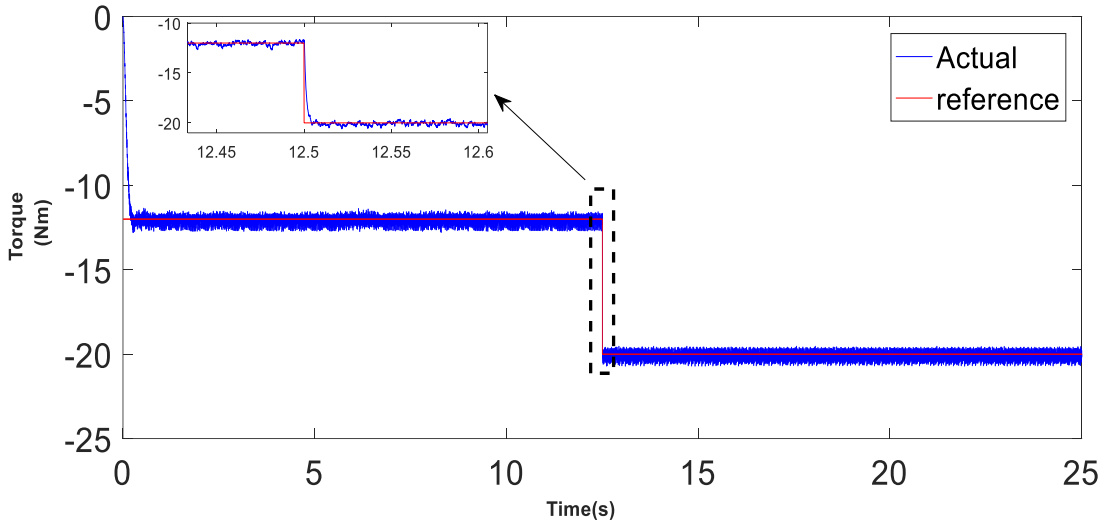

Fig. 28. Developed torque under MPCC (Nm)

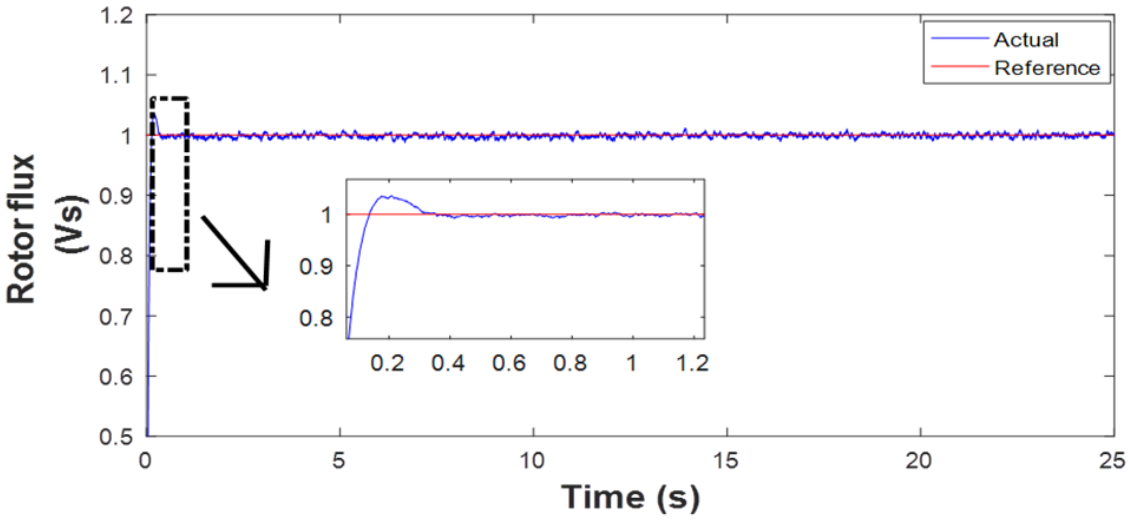

Fig. 29. Rotor flux under MPCC (Vs)

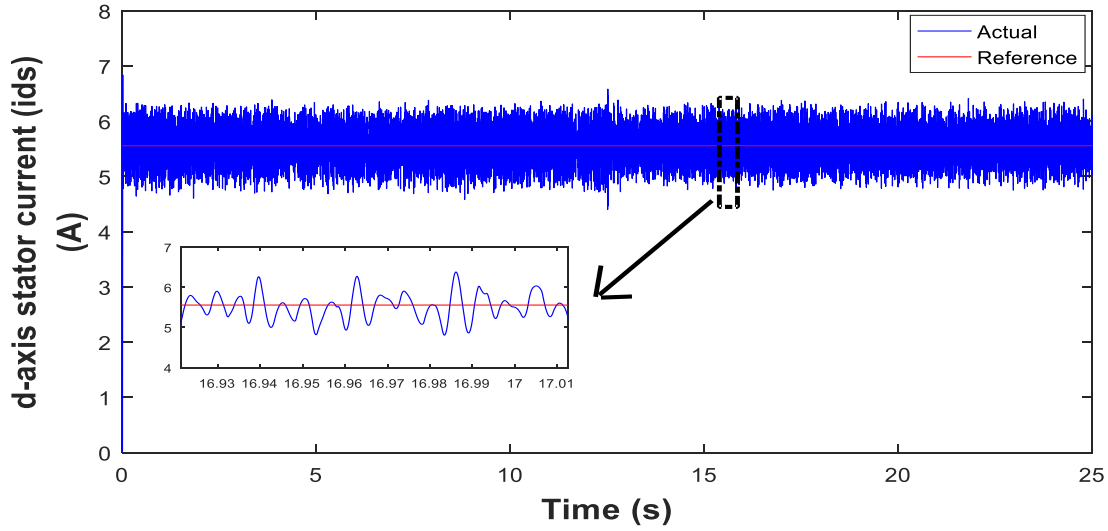

Fig. 30. d-axis stator current (i_{ds}) under MPCC (A)

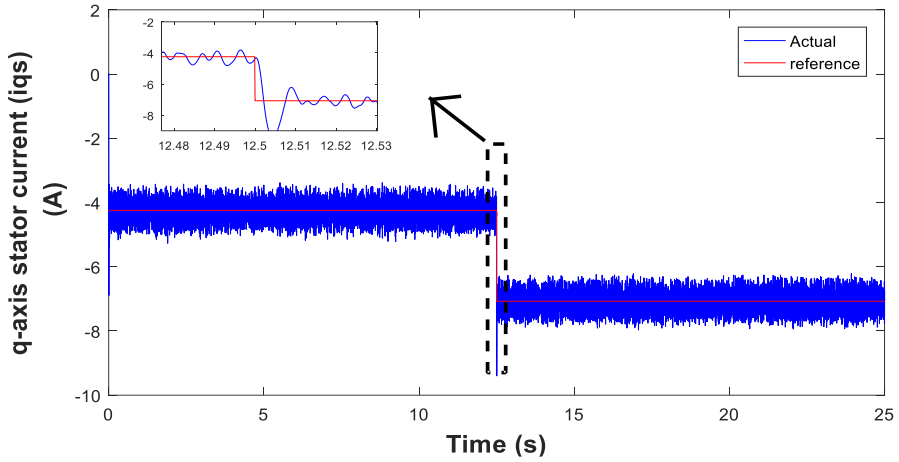

Fig. 31. q-axis stator current (i_{qs}) under MPCC

4.3. Testing with MPDTC Technique

The IG's performance was tested with the MPDTC technique, and the results for operating condition is respectively shown in Fig. 32 – Fig. 40, which illustrate that the actual values of the powers, torque, and rotor flux follow their references with a dynamic response faster than that of the MPCC and FOC principles, as the dynamic response of MPDTC is faster than the that of MPCC by 6% and faster than FOC by 11%. but unfortunately, it has more ripples than the MPCC and FOC techniques as it's cost function depend on w_f which inaccurate selection of it increase ripples, and torque & flux depend on generator parameter which any reflection of this parameters also increases ripples.

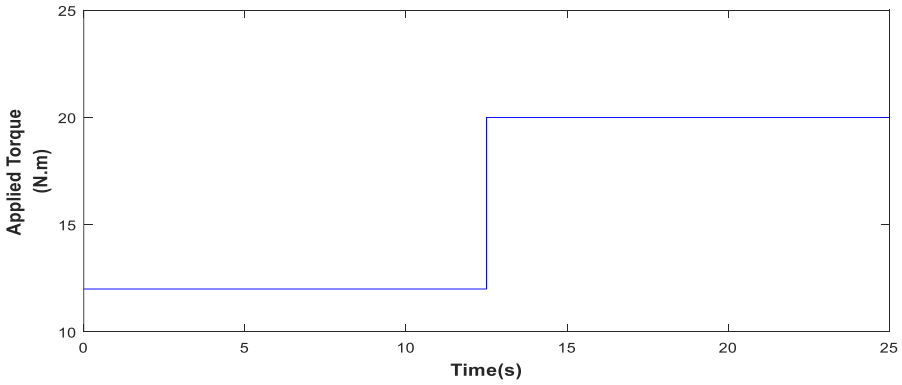

Fig. 32. Applied mechanical torque from prime mover (Nm)

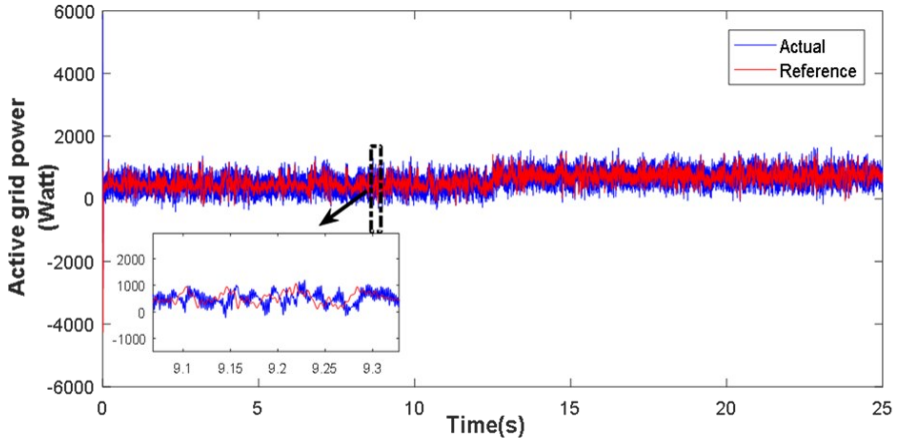

Fig. 33. Active grid power under MPDTC (Watt)

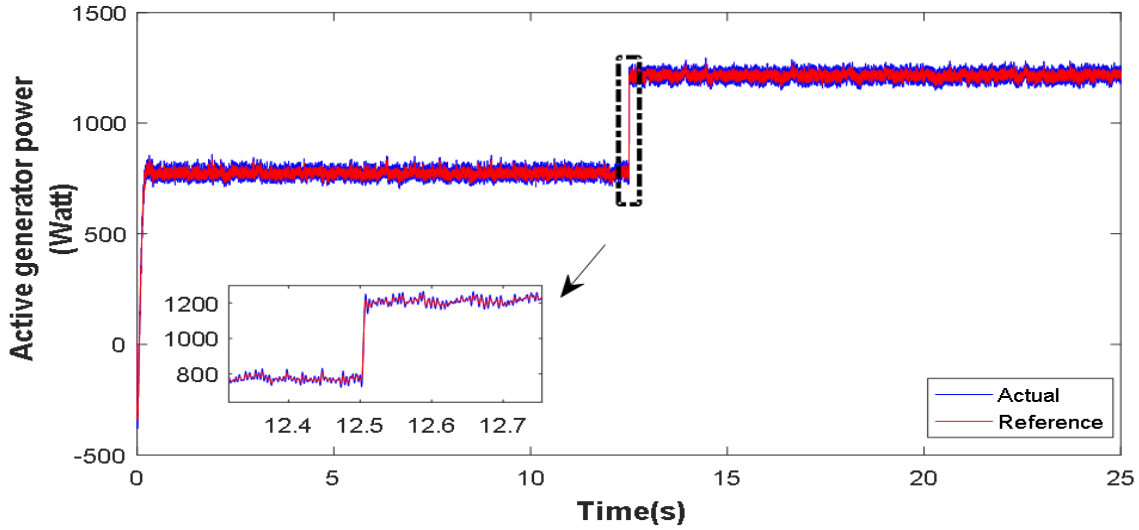

Fig. 34. Active generator power under MPDTC (Watt)

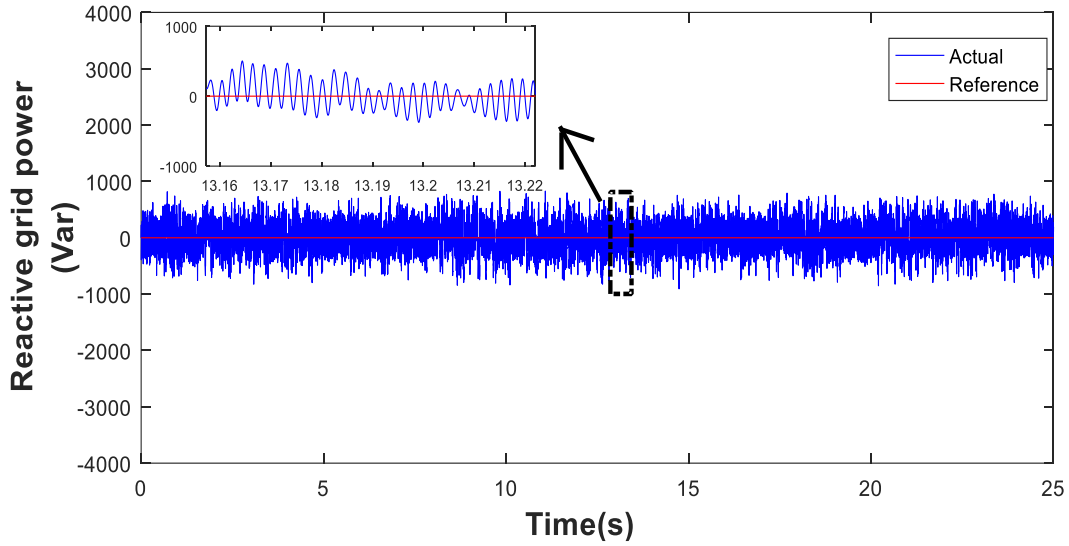

Fig. 35. Reactive grid power under MPDTC (Var)

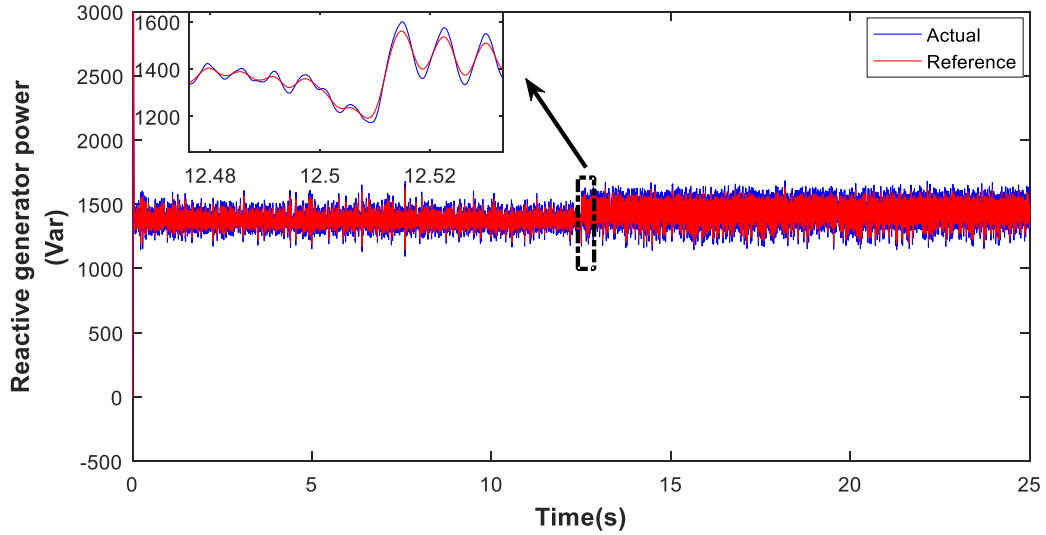

Fig. 36. Reactive generator power under MPDTC (Var)

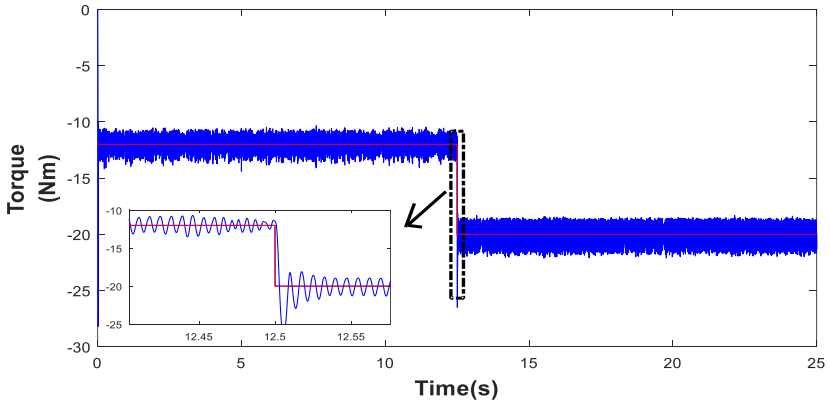

Fig. 37. Developed torque under MPDTC (Nm)

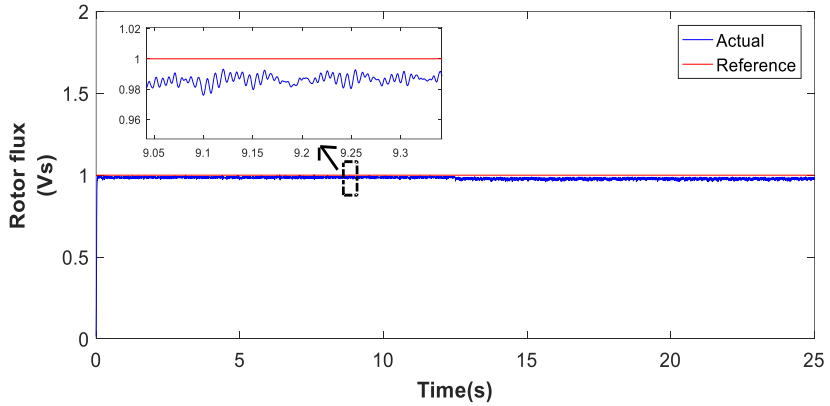

Fig. 38. Rotor flux under MPDTC (Vs)

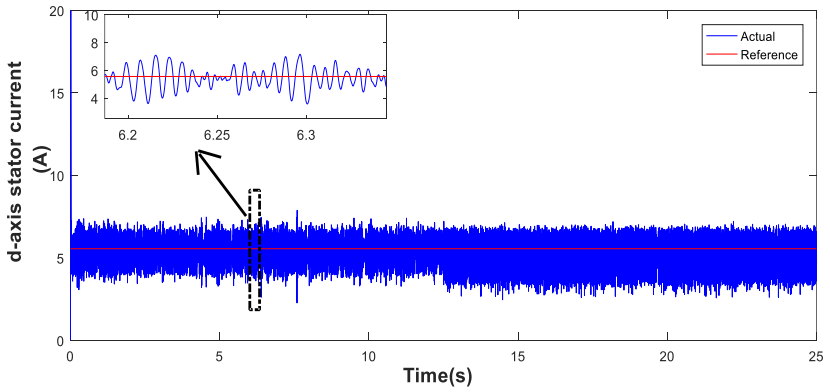

Fig. 39. d-axis stator current (i_{ds}) under MPDTC (A)

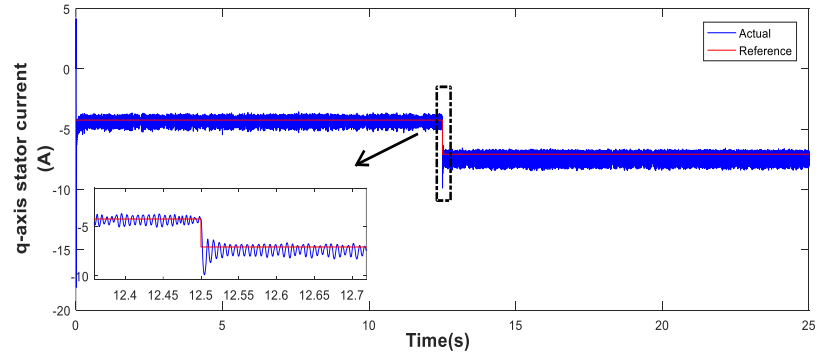

Fig. 40. q-axis stator current (i_{qs}) under MPDTC (A)

4.4. Testing with Proposed PVC

The IG's performance was tested with the proposed PVC technique, and the results are shown in Fig. 41 to Fig. 49 for the varying applied mechanical torque. These results prove and confirm that the proposed PVC control system has successfully achieved its targets, as the actual estimated values of the powers, torque, and rotor flux follow their references with high precision in the operating condition. Furthermore, the ripples content is effectively suppressed compared to the values under MPDTC and MPCC. In addition, the dynamic response of PVC is the fastest in comparison with that of the MPDTC, MPCC, and FOC techniques. As seen in Fig. 49, the q-axis component of the generator stator current change with changes in power and applied mechanical torque, while the d-axis component in Fig. 48 stays unchanged.

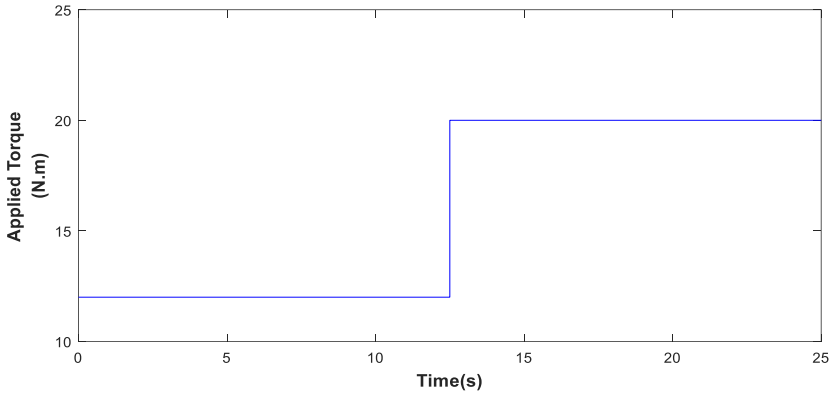

Fig. 41. Applied mechanical torque from prime mover (Nm)

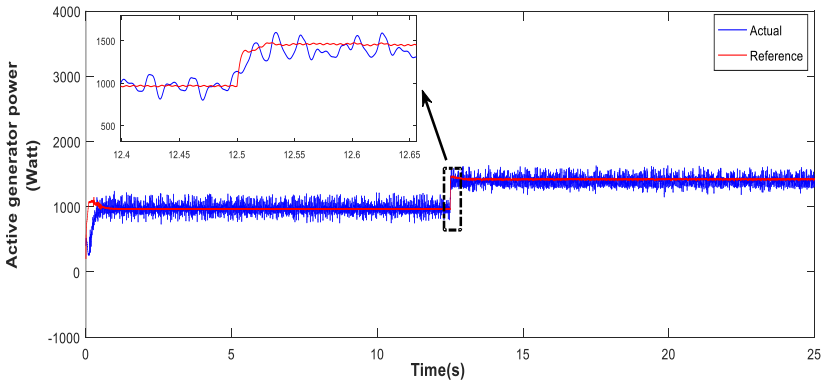

Fig. 42. Active generator power under PVC (Watt)

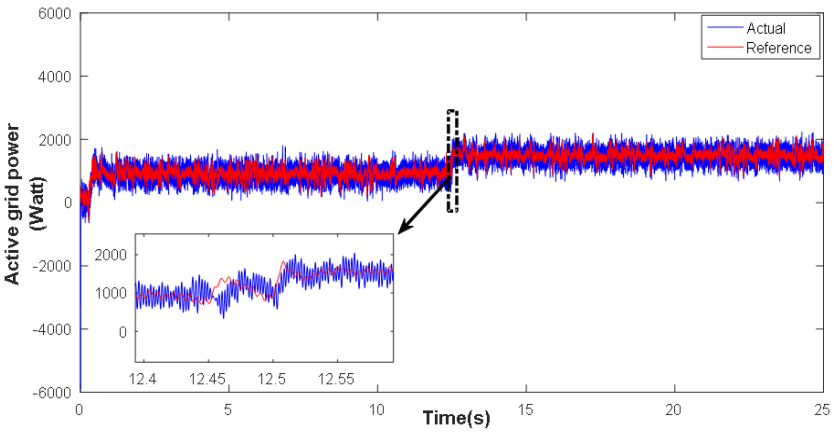

Fig. 43. Active grid power under PVC (Watt)

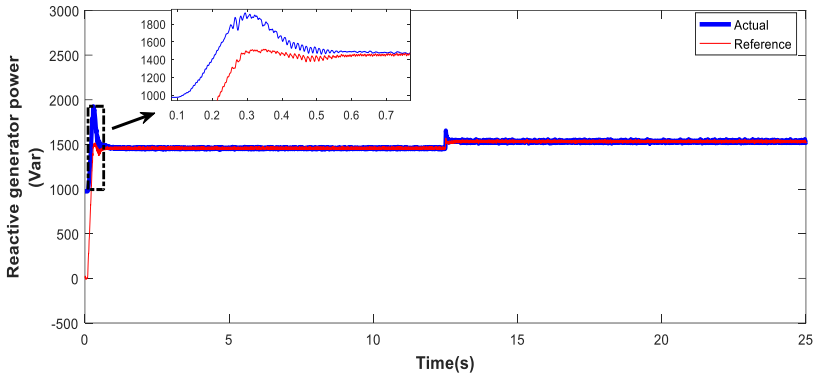

Fig. 44. Reactive generator power under PVC (Var)

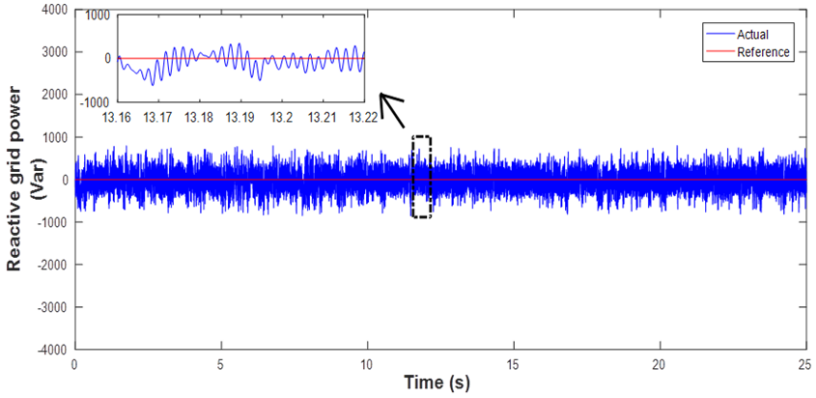

Fig. 45. Reactive grid power under PVC (Var)

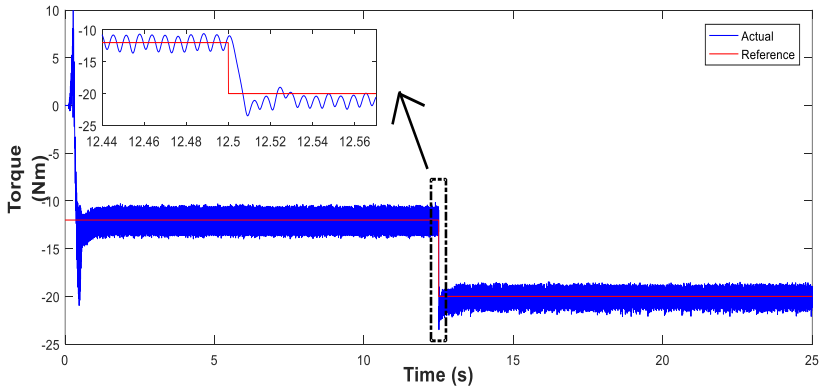

Fig. 46. Developed torque under PVC (Nm)

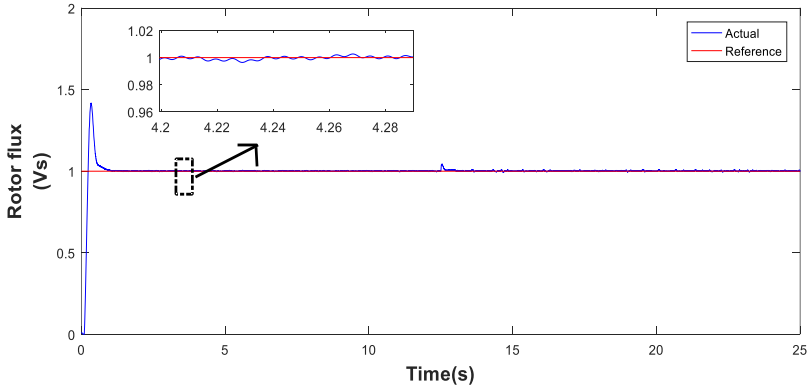

Fig. 47. Rotor flux under PVC (Vs)

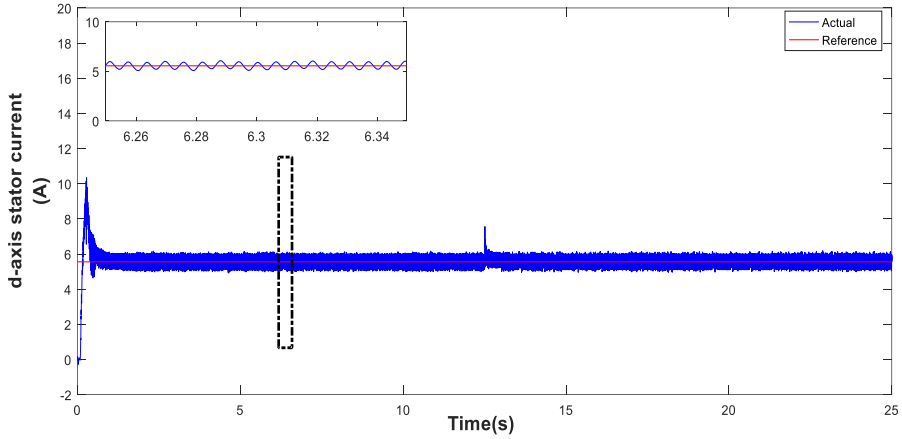

Fig. 48. d-axis stator current (i_{ds}) under PVC (A)

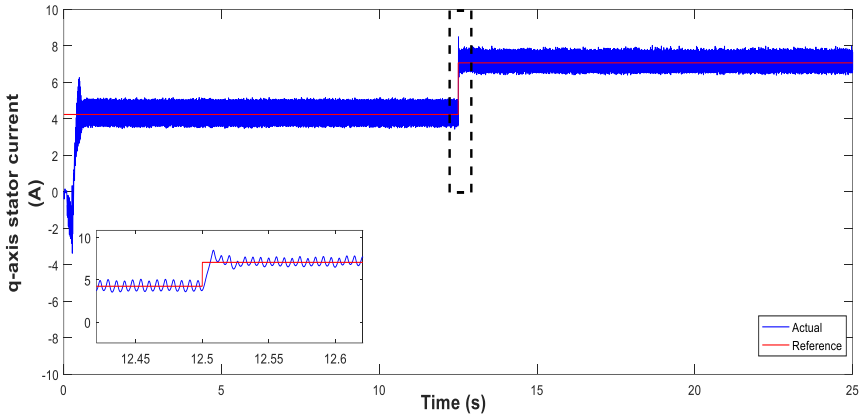

Fig. 49. Q-axis stator current (i_{qs}) under PVC (A)

4.5. Comparison Study

In order to identify the control technique that will work best with the SEIG, a comparison of the dynamic performance of the SEIG under the four control techniques (FOC, MPCC, MPDTC and PVC) for MSC and MPCC for GSC was completed. In terms of ripples, the effectiveness of the control was evaluated. The dynamic response time, ripple content and number of commutations were used to assess the effectiveness of the control.

The results are shown in Fig. 50 to Fig. 53, which outline the active power, reactive power for varying applied mechanical torque confirming that the PVC design has the least amount of ripples when compared to the other designs. Furthermore, Fig. 50 to Fig. 53 validates the accuracy of the control systems as the active power follows the applied mechanical torque while the reactive power is kept at zero. Fig. 54 to Fig. 57 illustrate the generated currents under FOC, MPCC, MPDTC and the proposed PVC control, respectively. These Fig. 54 to Fig. 57 demonstrate that the PVC algorithm is effective because it exhibits the fewest current harmonics when compared to the other algorithms.

With the help of the results, Table 1 compares the response times for each technique to show which one has the quickest dynamic response and, as a result, the shorter response times. The controlled variables in PVC are the voltage vectors, which are the closest electrical value applied to the machine windings, as shown in Table 1. As can be seen, the actual values under the suggested PVC technique demonstrate a quicker response time in contrast to the other control as it's time response is less than that of the FOC by 15%, MPCC by 9%, and MPDTC by 4%. So, the system with a faster time response, can track dynamic changes more effectively which improves accuracy

and performance. A quick time response can increase a system's stability and enable it to follow desired trajectories or make accurate motions in applications like motion control or robotics. The system can quickly achieve and maintain the optimal operating conditions by shortening the time it takes for it to react to changes or disruptions. In applications like power systems, control systems, and feedback control loops, where stability is crucial.

Table 1. Response time taken by the active and reactive powers to reach to their reference's values

Technique	Time taken by Active Generator Power	Time taken by Active Grid Power	Time taken by Reactive Generator Power	Time taken by Reactive Grid Power
FOC	410ms	213ms	314ms	500ms
MPCC	386.6ms	162ms	300ms	8.5ms
MPDTC	363ms	135ms	281ms	7.1ms
PVC	352ms	124ms	267ms	3.5ms

Table 2 compares the ripple content of the four concepts and shows that the PVC technique has less ripple content than the MPCC approach. As the ripples are reduced by 43% when compared to the MPDTC-used one and by 30% when compared to MPCC. As Commutations involve switching actions and can introduce electrical stresses and wear on the generator's components, such as the power electronics devices and the rotor windings. By minimizing the number of commutations, the stress on these components is reduced, leading to improved reliability and longevity of the SEIG. This is especially important in applications where the generator operates for long durations or under harsh environmental conditions. Also, Commutations in SEIGs can lead to the generation of harmonics and electromagnetic interference, which can affect the performance of other equipment connected to the same electrical system. By minimizing the number of commutations, the level of harmonics and EMI can be reduced, resulting in improved power quality and the avoidance of potential interference with sensitive equipment.

Table 2. Generator and Grid powers ripples (deviation from reference signals)

	MPDTC	MPCC	PVC
Generator active power ripples	±42.75W	±35W	±24.5W
Generator Reactive power ripples	±32.5Var	±15.5Var	±3.85Var
Grid active power ripples	±171.5W	±126.5 W	±97W
Grid reactive power ripples	±158.75Var	±153.5Var	±151.3Var

Table 3 compares the four controllers in terms of the number of commutations and the results show that the PVC has the fewest commutations, as it produces 38% fewer commutations than MPCC and 40% fewer commutations than MPDTC. So, it makes a significant contribution to lowering the computational burden, which is regarded as one of the main challenges of predictive control schemes. Where each commutation in an SEIG results in power losses due to switching actions. By reducing the number of commutations, the overall efficiency of the generator can be improved. This is particularly relevant in SEIG applications where energy conversion efficiency is crucial, such as renewable energy systems where every kilowatt-hour counts. Thus, it can be concluded that the proposed PVC technique is the best control method to be used with the SEIG because it achieves system simplification, has the fastest dynamic response in comparison to the MPCC, MPDTC, and FOC principles, and has a lower ripple content than the MPCC and MPDTC approaches. So, generator's efficiency and dependability both increased as a result of its better performance. While PVC offers several advantages as mentioned above, it also has certain limitations that should be taken into consideration. Here are some limitations of the PVC method in SEIG control:

1. Voltage Regulation Only: PVC primarily focuses on regulating the voltage at the GSC output. It does not directly address other important control aspects, such as frequency control or power

factor correction. Additional control strategies or techniques may be required to handle these aspects separately.

2. As the generation of voltage references is obtained using designed PI regulators whose operation is sensitive to model mismatch between the predictive model and the actual SEIG system. Precise tuning of the coefficients may be necessary to address model uncertainties and ensure stable operation.
3. However, of the utilization of FCS principle by the designed PVC and which simplifies the complete system and reduces the commutation, but on the other hand the fixed switching frequency operation cannot be ensured.

In brief, proper system design, model validation, robustness considerations, and real-time implementation techniques can help mitigate these limitations and enhance the overall control performance.

Table 3. Number of commutations for the four controllers

Technique	Number of commutations
MPCC	25680
MPDTC	26150
PVC	15910

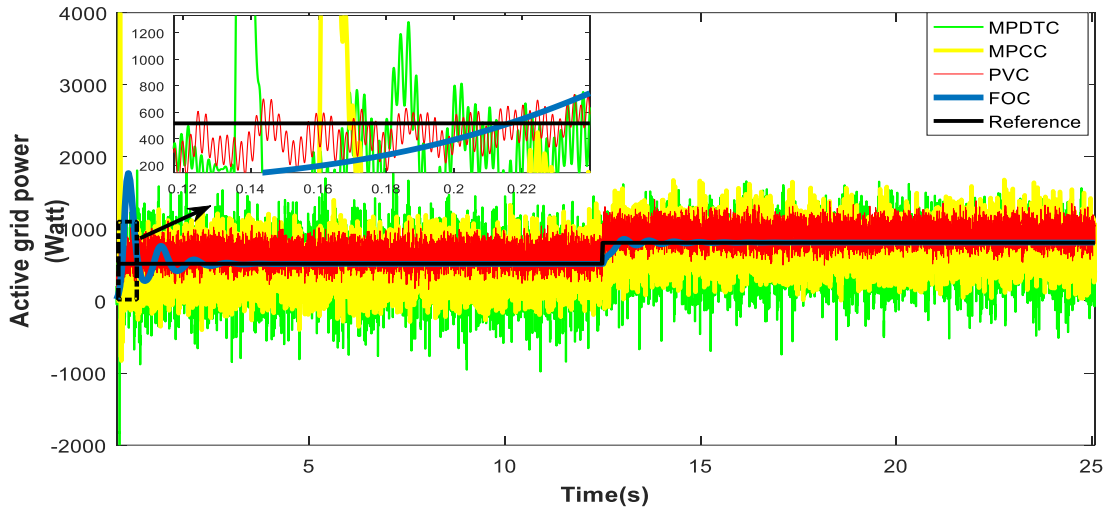

Fig. 50. Comparison between active grid powers of four techniques (W)

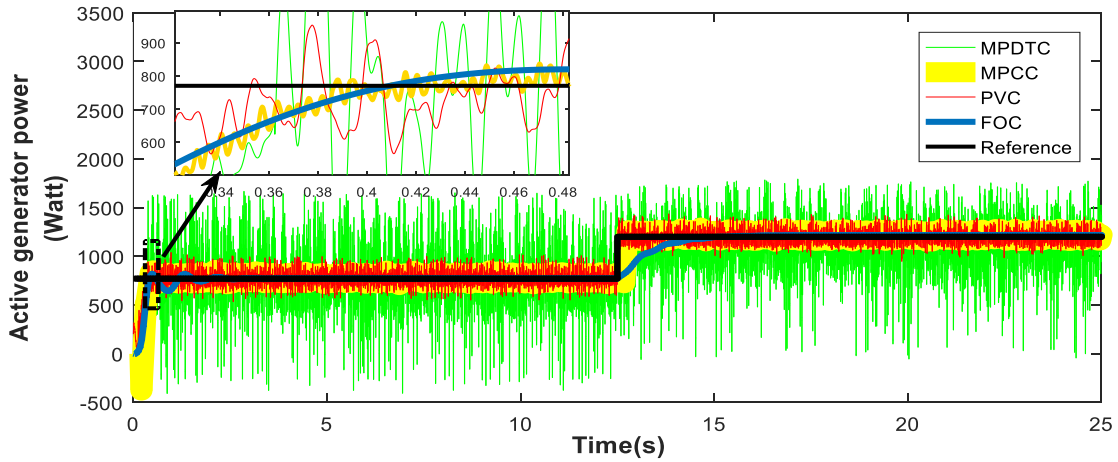

Fig. 51. Comparison between active generator powers of four techniques (W)

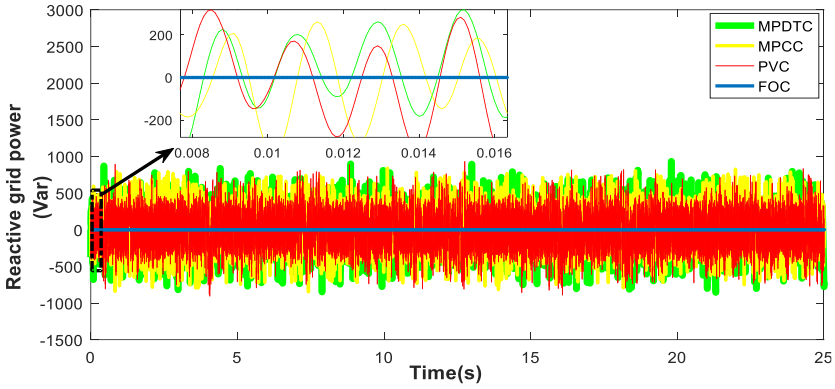

Fig. 52. Comparison between reactive grid powers of four techniques (Var)

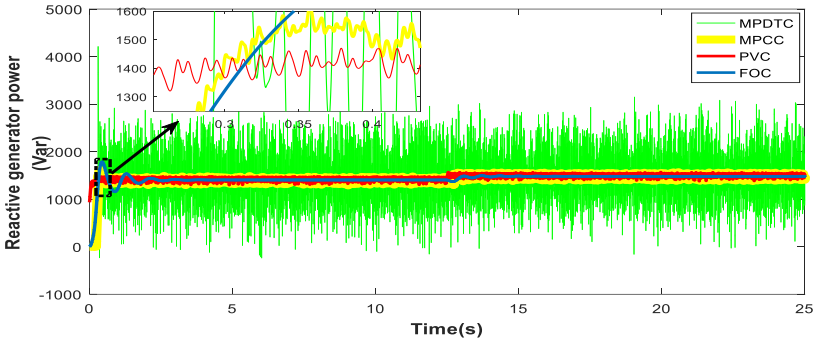

Fig. 53. Comparison between reactive generator powers of four techniques (Var)

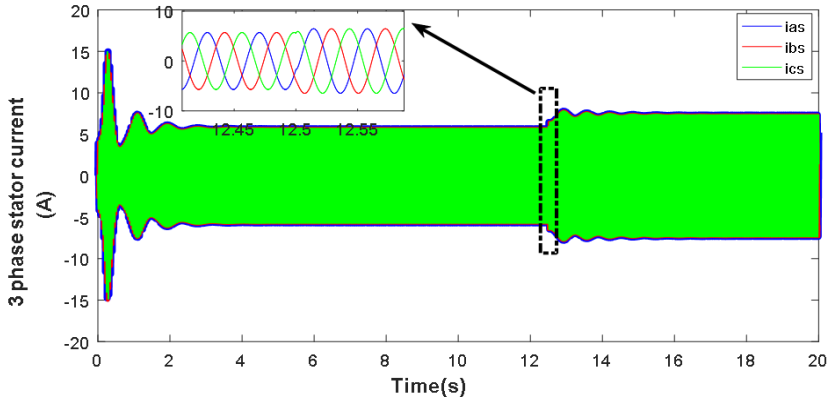

Fig. 54. Generator currents under FOC (A)

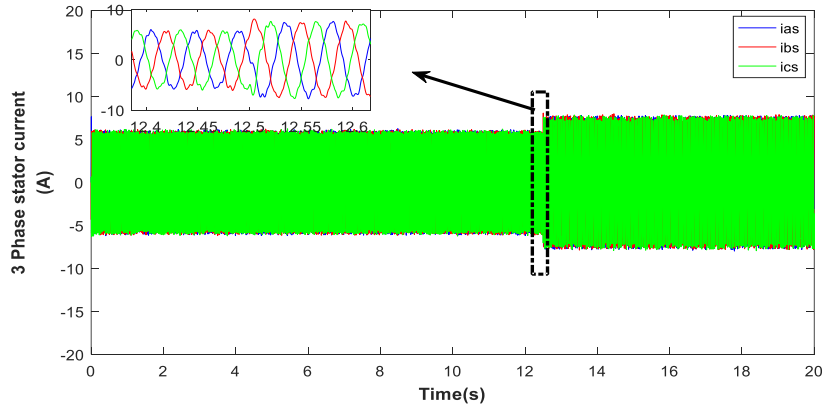

Fig. 55. Generator currents under MPCC (A)

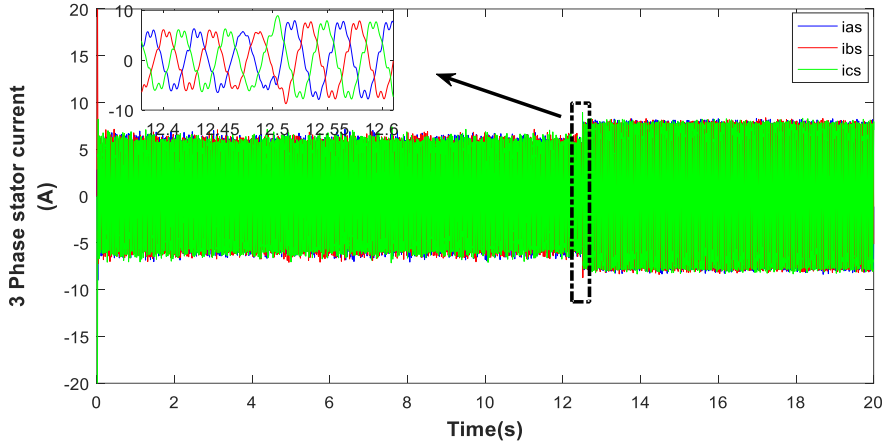

Fig. 56. Generator currents under MPDTC (A)

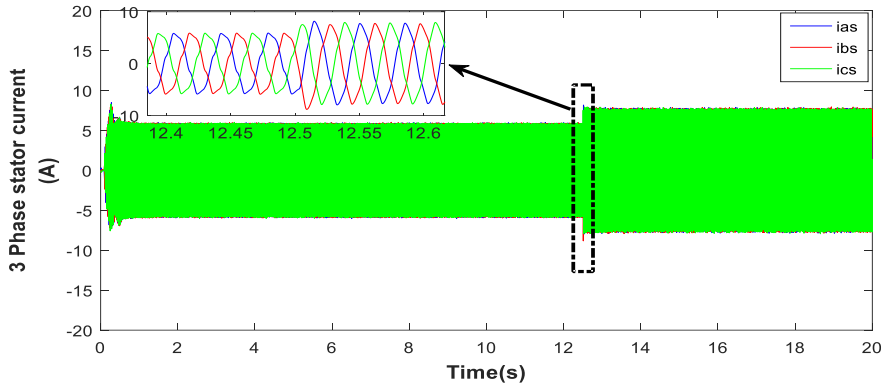

Fig. 57. Generator currents under PVC (A)

5. Conclusion

A comprehensive examination of the dynamic performance is provided for a SEIG operating at varying mechanical torque applied. Field oriented control (FOC), model predictive current control (MPCC), and model predictive direct torque control (MPDTC) systems are contrasted with the suggested (PVC) system. The suggested PVC has a number of benefits. For example, it uses a very simple cost function because it does not include a weighting factor or any other variables that need to be estimated. The cost function, which is made up of the absolute errors between the reference and actual values of the stator voltage component, greatly reduces the complexity required by the predictive controller. Since the inverter's switching signal can yield the actual voltage component required by the cost function after the finite control set (FCS) is adjusted, it is also possible to obtain the reference voltage component ($u_{ds}^{*}\ and\ u_{qs}^{*}$) through a reference method, which minimizes the number of commutations. The acquired findings demonstrate the effectiveness of the suggested PVC, as evidenced by the reduction of ripples by 43% compared to the MPDTC-used one and by 30% compared to MPCC. PVC's temporal response also differs by 15%, 9%, and 4% from those of the FOC, MPCC, and MPDTC, respectively. Increased system stability can be attributed to quicker reaction times and reduced ripple content. Reducing the time, it takes for the system to react to modifications or disruptions, the system can get to the desired operating conditions and stay there fast. This is crucial in applications like power systems, control systems, and feedback control loops where stability is a key component. Apart from that, PVC generates 38% fewer commutations than MPCC and 40% fewer commutations than MPDTC. Reducing torque ripple is a crucial prerequisite to lowering shaft variation and averting the mechanical issue. By enabling smoother and more consistent power injection, lowering grid instability, and raising overall grid stability and efficiency,

the PVC method, therefore, makes it easier for SEIGs to be integrated into the grid and increases their dependability, efficiency, and flexibility in response to changing industry demands and grid conditions. By taking into account the design of each generator, the suggested predictive voltage control can be utilized with different types of generators utilized in renewable energy systems, such as synchronous and double field induction generators.

Appendix A

Table A.1. SEIG and control system parameters

Parameters	Value
R_s	1.66 Ω
R_r	2.75 Ω
L_s	0.191 H
L_r	0.191 H
L_m	0.18 H
J	0.0099 kg.m^2
P	2
T_s	0.0001s
K_p and K_i (rotor current regulators)	8.3036, 55.3036
Operating frequency	50
U_{dc}	400V
W_f (Weighting factor)	20
Rated power	55 kW

Abbreviations and Symbols

SEIG	Self-Excited Induction generator	PC	Predictive control
FOC	Field oriented control	GSC	grid side converter
MPC	Model predictive control	MSC	machine side converter
MPDTC	Model predictive direct torque control	DC	Direct current
MPCC	Model predictive current control	R	Generator stator resistance
PVC	Predictive voltage control	L_s	Generator stator inductance
DTC	Direct torque control	ω_e	Angular frequency of the grid
DPC	Direct power control	P	Pole pairs number
SMC	sliding mode control	T_s	Sampling time
ANN	Artificial neural network	w_f	Weighting factor
IRFO	Indirect rotor field-oriented	u_{ds}& u_{qs}	actual d-q stator voltage component
FL	Fuzzy logic	u_{ds}^* & u_{qs}^*	reference d-q stator voltage component
API	Adaptive proportional-integral	Ψ_{ds}&Ψ_{qs}	d-q stator flux component
WECS	Wind energy conversion system	Ψ_{dr}&Ψ_{qr}	d-q rotor flux component
SVPWM	Space vector pulse width modulation	ω_g	angular frequency
FCS	Finite control set	i_{df} &i_{qf}	d-q components of the filter current
(RSCC	Rotor side connected converter	OLTF	Open-loop transfer function
GSCC	Grid Side Connected Converter	PLL	Phase locked loop
SPWM	Sinusoidal Pulse Width Modulation		

Author Contribution: All authors contributed equally to the main contributor to this paper. All authors read and approved the final paper.

Funding: This research received no external funding.

Conflicts of Interest: The authors declare no conflicts of interest.

References

[1] J. R. Andrade and R. J. Bessa, "Improving renewable energy forecasting with a grid of numerical weather predictions," *IEEE Transactions on Sustainable Energy*, vol. 8, no. 4, pp. 1571-1580, 2017, https://doi.org/10.1109/TSTE.2017.2694340.

[2] P. Siano, P. Chen, Z. Chen, and A. Piccolo, "Evaluating maximum wind energy exploitation in active distribution networks," *IET generation, transmission & distribution*, vol. 4, no. 5, pp. 598-608, 2010, https://doi.org/10.1049/iet-gtd.2009.0548.

[3] M. A. Mossa, O. Gam, and N. Bianchi, "Dynamic performance enhancement of a renewable energy system for grid connection and stand-alone operation with battery storage," *Energies*, vol. 15, no. 3, p. 1002, 2022, https://doi.org/10.3390/en15031002.

[4] S. Y. Yip, H. S. Che, C. P. Tan, and W. T. Chong, "A Lookup Table Model Predictive Direct Torque Control of Permanent-Magnet Synchronous Generator Based on Vienna Rectifier," *in IEEE Journal of Emerging and Selected Topics in Power Electronics*, vol. 8, no. 2, pp. 1208-1222, 2020, https://doi.org/10.1109/JESTPE.2019.2900917.

[5] P. J. dos Santos Neto, A. Cecílio Pinto, d. S. B. Tárcio André, and E. Ruppert Filho, "A Proposal to Control Active and Reactive Power in Distributed Generation Systems Using Small Wind Turbines," in *IEEE Latin America Transactions*, vol. 18, no. 10, pp. 1699-1706, 2020, https://doi.org/10.1109/TLA.2020.9387640.

[6] M. A. Mossa and S. Bolognani, "Predictive Power Control for a Linearized Doubly Fed Induction Generator Model," *2019 21st International Middle East Power Systems Conference (MEPCON)*, pp. 250-257, 2019, https://doi.org/10.1109/MEPCON47431.2019.9008085.

[7] M. A. Mossa, O. Gam, N. Bianchi, and N. V. Quynh, "Enhanced Control and Power Management for a Renewable Energy-Based Water Pumping System," in *IEEE Access*, vol. 10, pp. 36028-36056, 2022, https://doi.org/10.1109/ACCESS.2022.3163530.

[8] M. G. Simoes and F. A. Farret. *Alternative energy systems: design and analysis with induction generators*. CRC press, 2007, https://books.google.co.id/books?id=aybNBQAAQBAJ.

[9] A. F. Zobaa and R. C. Bansal. *Handbook of renewable energy technology*. World Scientific.2011. https://doi.org/10.1142/7489.

[10] M. M. Mahmoud, M. M. Aly, H. S. Salma, and A. M. M. Abdel-Rahim, "Dynamic evaluation of optimization techniques–based proportional–integral controller for wind-driven permanent magnet synchronous generator," *Wind Eng*, vol. 45, pp. 696–709, 2020, https://doi.org/10.1177/0309524X20930421.

[11] R. C. Bansal, "Three-phase self-excited induction generators: an overview," *IEEE transactions on energy conversion*, vol. 20, no. 2, pp. 292-299, 2005, https://doi.org/10.1109/TEC.2004.842395.

[12] G. M. Cocco, C. A. de Souza, F. B. Grigoletto, R. F. de Camargo, and F. E. Bisogno, "Model Predictive Control for Voltage Regulation of Standalone Self-Excited Induction Generator," *Simpósio Brasileiro de Sistemas Elétricos-SBSE*, vol. 2, no. 1, 2022, https://doi.org/10.20906/sbse.v2i1.3107.

[13] G. Kenne, C. T. Sanjong, and E. M. Nfah, "Adaptive PI control strategy for a self-excited induction generator driven by a variable speed wind turbine," *Journal of Circuits, Systems and Computers*, vol. 26, no. 2, p. 1750024, 2017, https://doi.org/10.1142/S0218126617500244.

[14] L. Bigarelli, M. di Benedetto, A. Lidozzi, L. Solero, S. A. Odhano, and P. Zanchetta, "PWM-Based Optimal Model Predictive Control for Variable Speed Generating Units," in *IEEE Transactions on Industry Applications*, vol. 56, no. 1, pp. 541-550, 2020, https://doi.org/10.1109/TIA.2019.2955662.

[15] H. S. Timorabadi, "Voltage source inverter for voltage and frequency control of a stand-alone self-excited induction generator," In *2006 Canadian Conference on Electrical and Computer Engineering*, pp. 2241-2244, 2006, https://doi.org/10.1109/CCECE.2006.277508.

[16] H. Echeikh, M. A. Mossa, N. V. Quynh, A. A. Ahmed, and H. H. Alhelou, "Enhancement of induction motor dynamics using a novel sensorless predictive control algorithm," *Energies*, vol. 14, no. 14, p. 4377, 2021, https://doi.org/10.3390/en14144377.

[17] A. Kishore, R. C. Prasad, and B. M. Karan, "Matlab Simulink based DQ modeling and dynamic characteristics of three phase self-excited induction generator," In *Progress in electromagnetics research symposium*, pp. 312-316, 2006, https://doi.org/10.2529/PIERS050905011004.

[18] G. S. Kumar and A. Kishore, "A generalized dynamic modeling and analysis of self-excited induction generator using state-space approach with ANN-model of magnetizing inductance," In *2006 IEEE International Conference on Industrial Technology*, pp. 2698-2703, 2006, https://doi.org/10.1109/ICIT.2006.372622.

[19] S. Vadhera and K. S. Sandhu, "Constant voltage operation of self excited induction generator using optimization tools," *International journal of energy and environment*, vol. 2, no. 4, pp. 191-198, 2008, https://www.naun.org/main/NAUN/energyenvironment/ee-62.pdf.

[20] K. Idjdarene, D. Rekioua, T. Rekioua, and A. Tounzi, "Vector control of autonomous induction generator taking saturation effect into account. Energy Conversion and Management, vol. 49, no. 10, pp. 2609-2617, 2008, https://doi.org/10.1016/j.enconman.2008.05.014.

[21] P. R. U. Guazzelli, W. C. de Andrade Pereira, C. M. R. de Oliveira, A. G. de Castro, and M. L. de Aguiar, "Weighting Factors Optimization of Predictive Torque Control of Induction Motor by Multiobjective Genetic Algorithm," in *IEEE Transactions on Power Electronics*, vol. 34, no. 7, pp. 6628-6638, 2019, https://doi.org/10.1109/TPEL.2018.2834304.

[22] G. Kenne, C. T. Sanjong, and E. M. Nfah, "Adaptive PI control strategy for a self-excited induction generator driven by a variable speed wind turbine," *Journal of Circuits, Systems and Computers*, vol. 26, no. 2, p. 1750024, 2017, https://doi.org/10.1142/S0218126617500244.

[23] M. Bašić, D. Vukadinović, and M. Polić, "Fuzzy DC-voltage controller for a vector controlled stand-alone induction generator," *International Journal of Circuits, Systems and Signal Processing*, vol. 7, no. 3, pp. 181-190, 2013, https://www.naun.org/main/NAUN/circuitssystemssignal/c052001-251.pdf.

[24] A. B. Jadhav, Y. Korsegaonkar, S. H. Pawar, and G. Buttanwad, "A comprehensive study of variable power to fixed power conversion of SEIG using power converter," In *2017 International Conference on Innovations in Information*, pp. 1-4, 2017, https://doi.org/10.1109/ICIIECS.2017.8276050.

[25] K. Premalatha, S. Vasantharathna, and T. Dhivyaah, "Self-excitation system for control of wind turbine driven induction generator using direct torque control," *Journal of Vibration and Control*, vol. 22, no. 3, pp. 736-755, 2016, https://doi.org/10.1177/1077546314532669.

[26] T. Jin, X. Shen, T. Su, and R. C. Flesch, "Model predictive voltage control based on finite control set with computation time delay compensation for PV systems," *IEEE Transactions on Energy Conversion*, vol. 34, no. 1, pp. 330-338, 2018, https://doi.org/10.1109/TEC.2018.2876619.

[27] N. Kumar and G. Dyanamina, "Comparative Studies of Grid-Connected SEIG-Based WECS Using a Different Type of Control Technique," In *2023 5th International Conference on Energy, Power and Environment: Towards Flexible Green Energy Technologies (ICEPE)*, pp. 1-6, 2023, https://doi.org/10.1109/ICEPE57949.2023.10201631.

[28] S. G. Petkar and V. K. Thippiripati, "Enhanced predictive current control of PMSM drive with virtual voltage space vectors," *IEEE Journal of Emerging and Selected Topics in Industrial Electronics*, vol. 3, no. 3, pp. 834-844, 2021, https://doi.org/10.1109/JESTIE.2021.3105316.

[29] M. A. Mossa and S. Bolognani, "Effective model predictive current control for a sensorless IM drive," In *2017 IEEE International Symposium on Sensorless Control for Electrical Drives (SLED)*, pp. 37-42, 2017, https://doi.org/10.1109/SLED.2017.8078427.

[30] S. A. Davari, V. Nekoukar, C. Garcia, and J. Rodriguez, "Online Weighting Factor Optimization by Simplified Simulated Annealing for Finite Set Predictive Control," in *IEEE Transactions on Industrial Informatics*, vol. 17, no. 1, pp. 31-40, 2021, https://doi.org/10.1109/TII.2020.2981039.

[31] T. M. Masaud and P. K. Sen, "Modeling and analysis of self-excited induction generator for wind energy conversion," *2015 IEEE Power & Energy Society Innovative Smart Grid Technologies Conference (ISGT)*, pp. 1-5, 2015, https://doi.org/10.1109/ISGT.2015.7131901.

[32] D. Perduková, P. Palacký, P. Fedor, P. Bober, and V. Fedák, "Dynamic Identification of Rotor Magnetic Flux, Torque and Rotor Resistance of Induction Motor," in *IEEE Access*, vol. 8, pp. 142003-142015, 2020, https://doi.org/10.1109/ACCESS.2020.3013944.

[33] K. B. Bimal. *Modern power electronics and AC drives*. New Jersy: Prentice Hall, 2002.

[34] K. Idjdarene, D. Rekioua, T. Rekioua, and A. Tounzi, "Vector control of autonomous induction generator taking saturation effect into account," *Energy Conversion and Management*, vol. 49, no. 10, pp. 2609-2617, 2008, https://doi.org/10.1016/j.enconman.2008.05.014.

[35] S. Mohanty, S. Pati, S. K. Kar, and J. Gantayat, "Comparative Performance Analysis of PI and SMC based Electric Spring for Wind Penetrated Isolated System," *2022 IEEE India Council International Subsections Conference (INDISCON)*, pp. 1-6, 2022, https://doi.org/10.1109/INDISCON54605.2022.9862844.

[36] K. Berabez, F. Hamoudi, K. Idjdarene, and I. Hacini, "Fuzzy Logic PI controller based Direct Torque control of a Self-Excited Induction Generator through a three-level Rectifier," *Journal of Renewable Energies*, vol. 1, no. 1, pp. 1-12, 2023, https://revue.cder.dz/index.php/rer/article/view/1093.

[37] D. Giribabu, M. Das, and A. Kumar, "Comparative study of control strategies for the induction generators in wind energy conversion system," *Wind and Structures*, vol. 22, no. 6, pp. 635-662, 2016, https://doi.org/10.12989/was.2016.22.6.635.

[38] M. A. Mossa and S. Bolognani, "Effective sensorless model predictive direct torque control for a doubly fed induction machine," *2017 Nineteenth International Middle East Power Systems Conference (MEPCON)*, pp. 1201-1207, 2017, https://doi.org/10.1109/MEPCON.2017.8301335.

[39] M. A. Mossa and S. Bolognani, "Robust Predictive Current Control for a Sensorless IM Drive Based on Torque Angle Regulation," *2019 IEEE Conference on Power Electronics and Renewable Energy (CPERE)*, pp. 302-308, 2019, https://doi.org/10.1109/CPERE45374.2019.8980183.

[40] K. Xiahou, M. S. Li, Y. Liu, and Q. H. Wu, "Sensor Fault Tolerance Enhancement of DFIG.-WTs via Perturbation Observer-Based DPC and Two-Stage Kalman Filters," in *IEEE Transactions on Energy Conversion*, vol. 33, no. 2, pp. 483-495, 2018, https://doi.org/10.1109/TEC.2017.2771250.

[41] S. Hammadi, N. Hidouri, and L. Sbita, "A DTC SEIG drive scheme for an isolated wind turbine buck system," *2013 International Conference on Control, Decision and Information Technologies (CoDIT)*, , pp. 543-548, 2013, https://doi.org/10.1109/CoDIT.2013.6689602.

[42] M. A. Mossa, A. Saad Al-Sumaiti, T. Duc Do, and A. A. Zaki Diab, "Cost-Effective Predictive Flux Control for a Sensorless Doubly Fed Induction Generator," in *IEEE Access*, vol. 7, pp. 172606-172627, 2019, https://doi.org/10.1109/ACCESS.2019.2951361.

[43] H. Geng, L. Liu, and R. Li, "Synchronization and Reactive Current Support of PMSG-Based Wind Farm During Severe Grid Fault," in *IEEE Transactions on Sustainable Energy*, vol. 9, no. 4, pp. 1596-1604, 2018, https://doi.org/10.1109/TSTE.2018.2799197.

[44] C. T. S. Dagang, G. Kenne, and F. A. Muluh, "Fuzzy logic direct torque/power control for a self-excited induction generator driven by a variable wind speed turbine," *International Journal of Dynamics and Control*, vol. 9, pp. 1210-1222, 2021, https://doi.org/10.1007/s40435-020-00709-9.

[45] S. A. Deraz and F. A. Kader, "A new control strategy for a stand-alone self-excited induction generator driven by a variable speed wind turbine," *Renewable Energy*, vol. 51, pp. 263-273, 2013, https://doi.org/10.1016/j.renene.2012.09.010.

[46] K. B. Bimal. *Power electronics and motor drives: advances and trends*. Academic Press, 2020, https://doi.org/10.1016/B978-0-12-821360-5.00007-5.

[47] M. A. Mossa, T. Duc Do, A. Saad Al-Sumaiti, N. V. Quynh, and A. A. Z. Diab, "Effective Model Predictive Voltage Control for a Sensorless Doubly Fed Induction Generator," in *IEEE Canadian Journal of Electrical and Computer Engineering*, vol. 44, no. 1, pp. 50-64, 2021, https://doi.org/10.1109/ICJECE.2020.3018495.

[48] M. A. Mossa, O. Gam, and N. Bianchi, "Performance enhancement of a hybrid renewable energy system accompanied with energy storage unit using effective control system", *Int. J. Robot. Control. Syst.*, vol. 2, no. 1, pp. 140-171, 2022, https://doi.org/10.31763/ijrcs.v2i1.599.